A real-time deployable model predictive control-based cooperative platooning approach for connected and autonomous vehicles

Jian Wang [a,b], Siyuan Gong [c], Srinivas Peeta [d,1], Lili Lu[a]

[a]*Faculty of Maritime and Transportation, Ningbo University, China*
[b]*Lyles School of Civil Engineering, Purdue University, West Lafayette, IN 47907, United States*
[c]*School of Information Engineering, Chang'an University, Shanxi, Xi'an, China*
[d]*School of Civil and Environmental Engineering, and H. Milton Stewart School of Industrial and Systems Engineering, Georgia Institute of Technology, Atlanta, GA 30332, United States*

Abstract: Recently, model predictive control (MPC)-based platooning strategies have been developed for connected and autonomous vehicles (CAVs) to enhance traffic performance by enabling cooperation among vehicles in the platoon. However, they are not deployable in practice as they require the embedded optimal control problem to be solved instantaneously, with platoon size and prediction horizon duration compounding the intractability. Ignoring the computational requirements leads to control delays that can deteriorate platoon performance and cause collisions between vehicles. To address this critical gap, this study first proposes an idealized MPC-based cooperative control strategy for CAV platooning based on the strong assumption that the problem can be solved instantaneously. It also proposes a solution algorithm for the embedded optimal control problem to maximize platoon performance. It then develops two approaches to deploy the idealized strategy, labeled the deployable MPC (DMPC) and the DMPC with first-order approximation (DMPC-FOA). The DMPC approach reserves certain amount of time before each sampling time instant to estimate the optimal control decisions. Thereby, the estimated optimal control decisions can be executed by all the following vehicles at each sampling time instant to control their behavior. However, under the DMPC approach, the estimated optimal control decisions may deviate significantly from those of the idealized MPC strategy due to prediction error of the leading vehicle's state at the sampling time instant. The DMPC-FOA approach can significantly improve the estimation performance of the DMPC approach by capturing the impacts of the prediction error of the leading vehicle's state on the optimal control decisions. An analytical method is derived for the sensitivity analysis of the optimal control decisions. Further, stability analysis is performed for the idealized MPC strategy, and a sufficient condition is derived to ensure its asymptotic stability under certain conditions. Numerical experiments illustrate that the control decisions estimated by the DMPC-FOA approach are very close to those of the idealized MPC strategy under different traffic flow scenarios. Hence, DMPC-FOA can address the issue of control delay of the idealized MPC strategy effectively and can efficiently coordinate car-following behaviors of all CAVs in the platoon to dampen traffic oscillations. Thereby, it can be applied for real-time cooperative control of a CAV platoon.

Keywords: Connected and autonomous vehicles; deployable model predictive control approaches; sensitivity analysis; stability analysis

1. Introduction

Connected and autonomous vehicle (CAV) technologies provide disruptive and transformational

[1] Corresponding author. Tel.: +1 404-894-2243.
Email address: srinivas.peeta@ce.gatech.edu (S. Peeta)

opportunities for innovations toward intelligent transportation systems. Unlike human-driven vehicles, CAVs have shorter reaction times, better knowledge of ambient traffic (in terms of speed, position, acceleration, etc.), and faster information processing speeds. These characteristics enable CAVs to form platoons to drive cooperatively on the road, in which a vehicle maintains a small and nearly constant headway with its preceding vehicle. Past studies suggest that vehicle platooning of CAVs can benefit transportation systems in many ways (Jia et al., 2015). It can increase road capacity, reduce energy consumption and tailpipe emissions, and facilitate vehicle-to-vehicle based applications (involving data sharing and dissemination) due to the relatively fixed positions of vehicles within a platoon.

In the literature, many adaptive cruise control (ACC) models and cooperative ACC (CACC) models have been proposed to control longitudinal car-following behavior of vehicles to enable efficient vehicle platooning. The ACC makes car-following decisions based on the preceding vehicle's information (speed and position) obtained through onboard sensors (e.g., VanderWerf et al., 2001; Hasebe et al., 2003; Kesting et al., 2008; Darbha and Rajagopal, 1999), while CACC makes car-following decisions with more information (speed, position and/or acceleration) from either a single vehicle or multiple vehicles in the platoon by leveraging connectivity technologies. The CACC models can improve the stability and efficiency of the ACC models by reducing the delay in responding to the preceding vehicle. According to Wang et al. (2014a), CACC models can be divided into two categories, the cooperative sensing-based models and the cooperative behavior-based models. The cooperative sensing-based models seek to optimize individual vehicle's performance using, for example, the immediate preceding vehicle's information (with acceleration) (Rajamani, R., Shladover, S.E. 2001, Desjardins and Chaib-draa, 2011), multiple preceding vehicles' information (Li et al., 2011; Jia and Ngoduy, 2016; Ge and Orosz, 2014; Ploeg et al., 2014) or the preceding-and-following vehicles' information (Zheng et al., 2016; Nakayama et al., 2001). It is important to note that the behaviors of vehicles controlled by these models are non-cooperative. That is, the control is not based on viewing a group of vehicles as an integrated system, which can deteriorate system (platoon) performance in terms of safety, mobility, energy consumption, etc.

To bridge this gap, recently, cooperative behavior-based CACC models have been proposed to coordinate the behaviors (accelerations or decelerations) of all of the following vehicles in a CAV platoon (e.g., Wang et al., 2014b; Zhou et al., 2017; Gong and Du, 2018). Most of these models are developed by leveraging the model predictive control (MPC) cooperative control approach. The MPC approach incorporates an optimal control problem to optimize the control decisions of the following vehicles in the platoon for some future period (labeled prediction horizon) to maximize the platoon performance based on the vehicles' state information at the current time. It has the flexibility to deal with multiple design criteria and constraints on state and control variables. Wang et al. (2014b) propose a MPC approach to coordinate the behaviors of all CAVs in a platoon to optimize a cost function reflecting different control objectives. Numerical applications illustrate that this approach can lead to smoother deceleration behavior and more responsive and agile acceleration behavior compared to non-cooperative controllers. Zhou et al. (2017) extend Wang et al. (2014b) by addressing the impacts of uncertainty in both system dynamics and sensor measurements on vehicle control. They propose a discrete Kalman filter to estimate the system state and a stochastic MPC approach to determine the optimal control. Gong and Du (2018) apply the MPC approach to coordinate multiple CAV platoons separated by human driven vehicles to enhance the smoothness and stability of the mixed flow platoon. Wang et al. (2019) provide

a detailed review of the recent CAV trajectory control methods.

While the aforementioned MPC-based cooperative control strategies can coordinate the car-following behaviors of CAVs in a platoon effectively, their real-time deployability requires that at each sampling time instant, the group of CAVs solve the embedded optimal control problem instantaneously (i.e., in much less than 0.1 seconds) to obtain the vehicles' control decisions based on their detected states (e.g., speed and positions) at that instant. These decisions then need to be executed to control the CAV platoon at the sampling time instant with no delay. However, this requirement cannot be satisfied in practice due to the computational time required by the CAVs to solve the optimal control problem. As pointed by Zhou et al. (2017), the computational time for solving the optimal control problem increases monotonically with the number of vehicles in the platoon and the prediction horizon. It can become intractable in real traffic systems due to the expansion of the dimensionality of state and control input spaces (Wang et al., 2016). Thereby, based on platoon size and prediction horizon length, the computational time of the optimal control problem can cause significant delay (labeled control delay) in the execution of the optimal control decisions for the CAV platoon. As the CAVs' states change dynamically, the control delay can significantly deteriorate performance and even induce vehicle collisions. This precludes these MPC-based cooperative control strategies for a CAV platoon from being applied in real-time.

Some recent studies have sought to reduce the control delay induced by the computational time to solve the optimal control problem embedded in MPC-based cooperative control strategies. Wang et al. (2016) propose a decentralized MPC strategy which considers cooperation among only two vehicles in a decoupled platoon system, which reduces the computational time substantially as only two vehicles' control decisions are optimized simultaneously. However, the performance of the CAV platoon cannot be enhanced to the fullest under this strategy as only two vehicles' behaviors are coordinated at the same time under a common objective. Further, the computational time for solving the optimal control problem can increase with the prediction horizon for even the decoupled platoon system. Gong and Du (2018) propose a distributed solution algorithm to reduce computational time by distributing the computational tasks among all CAVs in the platoon. However, the computational time of this algorithm can increase dramatically with platoon size and prediction horizon. Hence, these methods (e.g., Wang et al., 2016; Gong and Du, 2018) alleviate the issue of control delay of MPC-based cooperative control strategies to only a certain extent, but are still limited by platoon size and/or prediction horizon.

This study develops two real-time deployable MPC-based approaches that address the issue of the control delay at a fundamental level. In this study, the phrase "real-time deployable" refers to the capability that these approaches can overcome the control delay issue and can provide the optimal control decisions for all following vehicles in the platoon instantaneously at each sampling time instant. To do so, first, an idealized MPC-based cooperative control strategy is proposed by modifying the strategies proposed by Wang et al. (2014b) and Zhou et al. (2017). It can coordinate the behavior of all of the following CAVs in the platoon to maneuver them efficiently and safely on the idealized assumption that the embedded optimal control problem can be solved instantaneously. To relax this assumption, two deployable approaches, labeled the deployable MPC (DMPC) approach and the DMPC with first-order approximation (DMPC-FOA) approach, are proposed to address the issue of computational delay associated with solving the optimal control problem in the idealized MPC-based strategy. It should be noted that to enable efficient coordination of the car-following behaviors of all CAVs in the platoon,

such approaches need to accurately characterize the optimal control decisions of the idealized MPC-based strategy.

The DMPC approach reserves sufficient time before each sampling time instant to solve the optimal control problem so that the optimal control decisions can be obtained in advance to be executed at the corresponding sampling time instant with no delay. However, as the leading vehicle of a platoon needs to respond to the dynamics of the vehicles downstream of it, its behavior cannot be controlled and coordinated with those of the following vehicles in the platoon. Thereby, its position and speed at each sampling time instant need to be predicted ahead of that time, which is determined by the time reserved for computing. Hence, the optimal control decisions of the DMPC approach can deviate from that of the idealized MPC strategy due to error in predicting the leading vehicle's position and speed in advance. To address this problem, the DMPC-FOA approach is proposed to more accurately characterize the optimal control decisions of the idealized MPC strategy. Before each sampling instant, the DMPC-FOA approach reserves sufficient time to determine not only the optimal control decisions using the leading vehicle's predicted position and speed at the sampling time instant, but also the derivatives of the estimated optimal control decisions with respect to the leading vehicle's position and speed. Thereby, at the sampling time instant when the leading vehicle's actual position and speed are detected, the first-order Taylor approximation method can be applied to correct the estimated optimal control decisions for the following vehicles. Numerical experiments illustrate that the DMPC-FOA approach can address the issue of control delay while accurately estimating the optimal control decisions of the idealized MPC strategy.

The contributions of this study are fivefold. First, an idealized MPC strategy is proposed to coordinate the behaviors of the following vehicles in the platoon by modifying the control strategies proposed by Wang et al. (2014b) and Zhou et al. (2017). Further, a solution algorithm is proposed to solve the optimal control problem with both control constraints and pure state constraints in the idealized MPC strategy. A two-point boundary value problem is derived based on the necessary conditions for optimality to obtain the optimal control decisions to coordinate the behaviors of all vehicles in the platoon to maximize the platoon performance. Second, the study develops the DMPC-FOA approach that simultaneously addresses the control delay issue while accurately characterizing the optimal control decisions of the idealized MPC strategy. Thereby, it can be applied in real-time to efficiently coordinate the car-following behaviors of all CAVs in a platoon. Third, the method for sensitive analysis of the optimal control problem is analytically formulated. It can quantitatively measure the impact of parametric perturbations (e.g., perturbations of initial state of the leading vehicle) on the optimal control decisions and the platoon performance. Fourth, this study shows analytically that the derivatives of the optimal control decisions with respect to parametric perturbations are the same when the inequality constraints in the proposed optimal control problem (e.g., acceleration range constraints, speed range constraints, spacing headway constraints) are inactive in some traffic scenarios (e.g., uncongested traffic flow with mild acceleration and deceleration behavior of the leading vehicle). These results can be used as initial points in the algorithm to solve for these derivatives faster when the constraints in the optimal control problem are active in certain traffic scenarios (e.g., very congested flow). This enhances the real-time applicability of the proposed method. Fifth, an analytical method is provided for stability analysis of the idealized MPC strategy. It helps to identify the inputs of the parameters in the idealized MPC strategy to better dampen the oscillations in the platoon.

It is important to note that this study is fundamentally different from that of Wang et al. (2018),

which discusses a compensation strategy for sensor delay and actuator lag. The compensation strategy can account for the differences between the sensed kinematic states of all following vehicles and the actual ones at the sampling time instant by leveraging the optimal control decisions for all following vehicles in the last control cycle. However, in their study, the computational time for solving the optimal control problem is neglected. Thereby, they do not study the impacts of the prediction error of the leading vehicle's state at the sampling time instant on the optimal control decision. Note that the leading vehicle's behavior cannot be controlled. Thereby, unlike for the following vehicles in the platoon, the deviation between the predicted leading vehicle's state and the actual one at the sampling time instant cannot be compensated using the method proposed in Wang et al. (2018).

The remainder of this paper is organized as follows. The next section provides the analytical formulation of the idealized MPC cooperative control strategy for a CAV platoon and discusses the framework for the DMPC and DMPC-FOA approaches. Section 3 introduces the solution algorithm to solve the optimal control problem in the idealized MPC strategy. The method for the sensitivity analysis of the optimal control problem is presented in Section 4. Section 5 discusses the conditions for the stability of the idealized MPC strategy without inequality constraints. Section 6 discusses results of numerical experiments to compare the control performance of the idealized MPC strategy and the DMPC and DMPC-FOA approaches. The last section provides some concluding comments.

2. MPC approaches for longitudinal control of CAV platoon

2.1 An idealized MPC cooperative control strategy for a CAV platoon

This section presents an idealized MPC strategy to control the CAVs in a platoon cooperatively by modifying the control strategies developed by Wang et al. (2014b) and Zhou et al. (2017). It seeks to coordinate the behavior of all following vehicles to: (1) maintain a desired safe spacing (labeled equilibrium spacing) between two consecutive vehicles in a platoon, and reduce traffic flow oscillations in terms of spacing and speed changes, and (2) maximize the comfort of travelers in these vehicles by minimizing deceleration and acceleration. The details of the idealized MPC strategy are as follows.

Consider a stream of CAVs in a single highway lane as shown in Fig. 1. Let $0,1,2\cdots,n$ represent the CAVs in the platoon sequentially with 0 being the leading CAV and n being the tail CAV. The following assumptions will be used to design the longitudinal control of the CAV platoon:

1. All vehicles in the platoon are CAVs.
2. Two-way V2V communications exist between the leading vehicle and each of the following vehicles in the platoon (see Fig.1). Each following vehicle sends real-time information (speed and position) to the leading vehicle. The leading vehicle sends the computed optimal control decisions to each of the following vehicles to control their driving behavior.
3. All CAVs can sense their kinematic states (speed, position, etc.) accurately and can send that information to the leading vehicle of their platoon instantaneously.
4. The leading CAV computes and sends the optimal control decisions (i.e., accelerations and decelerations) to all of the following CAVs which implement these decisions.
5. The actuator delay is negligible; that is, vehicles can implement the control instantly.
6. The pavement of the highway lane is in good condition and longitudinal slope is negligible.

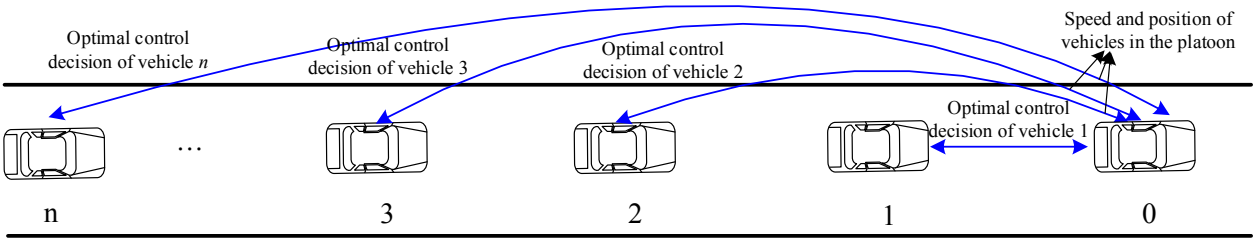

Fig. 1. A CAV platoon stream.

In this study, we treat a platoon of CAVs as an integrated system, in which vehicles within the platoon are controlled in a coordinated manner. Define the state of a follower vehicle i as $\left(s_i(t) - s_i^*(t), v_i(t) - v_{i-1}(t)\right)$, where $s_i(t)$ is the spacing of vehicle i with its predecessor vehicle at time t, $v_i(t)$ is the speed of vehicle i at time t, and $s_i^*(t)$ is the equilibrium spacing at time t. This study uses the constant time headway policy to determine the equilibrium spacing. Thereby, $s_i^*(t) = r_i^* \cdot v_i(t) + s_f$, where r_i^* is the constant time headway for vehicle i and s_f is the safe distance to the predecessor vehicle. For simplicity, the constant time headway for each follower vehicle in the platoon is assumed to be the same, i.e., $r_i^* = r^*, \forall i = 1,2,\cdots n$. Let $x_i(t) = s_i(t) - s_i^*(t), \forall i$ be the position error between the desired spacing and actual spacing of vehicle i from its predecessor vehicle at time t. Denote $y_i(t)$ as the speed difference of vehicle i from its predecessor vehicle at time t, i.e., $y_i(t) = v_i(t) - v_{i-1}(t)$. Denote $d_i(t)$ as the longitudinal position of CAV i in the platoon at time t. Then,

$$x_i(t) = d_{i-1}(t) - d_i(t) - r^* \cdot v_i(t) - s_f \tag{1}$$

and

$$\dot{x}_i(t) = v_{i-1}(t) - v_i(t) - r^* \cdot u_i(t) \tag{2a}$$

$$\dot{y}_i(t) = u_i(t) - u_{i-1}(t) \tag{2b}$$

where $\dot{x}_i(t)$ is the first-order derivative of position error of vehicle i from its predecessor vehicle with respect to time t. $\dot{y}_i(t)$ is the first-order derivative of speed difference of vehicle i from its predecessor vehicle with respect to time t. $u_i(t)$ is the acceleration of CAV i at time t.

Assume that the leading vehicle 0 travels at a constant speed. The spacing of vehicle $i, \forall i = 1,2,\cdots,n$ from its predecessor vehicle can then be expressed as:

$$s_i(t) = x_i(t) + r^* \cdot \left(v_0(t) + \sum_{j=1}^{i} y_j(t)\right) + s_f, \forall i = 1,2,\cdots,n \tag{3}$$

Denote $\mathbf{x}(t) = [x_1(t), x_2(t), \cdots, x_n(t)]^T$, $\mathbf{y}(t) = [y_1(t), y_2(t), \cdots, y_n(t)]^T$, and $\boldsymbol{u}(t) = [u_1(t), u_2(t), \cdots, u_n(t)]^T$. $\mathbf{x}(t)$ and $\mathbf{y}(t)$ are vectors of state variables. Then, the dynamics of the states (i.e., $\mathbf{x}$ and $\mathbf{y}$) are as follows:

$$\begin{bmatrix}\dot{\mathbf{x}}(t)\\ \dot{\mathbf{y}}(t)\end{bmatrix} = \underbrace{\begin{bmatrix}\mathbf{0}_n & -\boldsymbol{E}_n\\ \mathbf{0}_n & \mathbf{0}_n\end{bmatrix}}_{\boldsymbol{A}}\begin{bmatrix}\mathbf{x}(t)\\ \mathbf{y}(t)\end{bmatrix} + \underbrace{\begin{bmatrix}\mathbf{M}\\ \boldsymbol{S}\end{bmatrix}}_{\boldsymbol{B}} \cdot \boldsymbol{u}(t) \tag{4}$$

where $\dot{\mathbf{x}}(t)$ and $\dot{\mathbf{y}}(t)$ are first-order derivatives of $\mathbf{x}(t)$ and $\mathbf{y}(t)$ with respect to time t, $\mathbf{0}_n$ is the n-dimensional zero square matrix, and $\mathbf{M} = -r^* \cdot \boldsymbol{E}_n$, $\boldsymbol{E}_n$ is the n-dimensional identity matrix. Matrices $\boldsymbol{A}$ and $\boldsymbol{B}$ are defined in Eq. (4). The matrix $\boldsymbol{S}$ is:

$$\boldsymbol{S} = \begin{bmatrix} 1 & & & & \\ -1 & 1 & & & \\ & -1 & 1 & & \\ & & \ddots & \ddots & \\ & & & -1 & 1 \end{bmatrix}^{n\times n}$$

Following the elucidation of the state variables, the next step in developing the idealized MPC strategy is the conceptual illustration of its implementation framework and computational procedure, as shown in Figs. 2(a) and 2(b), respectively. In Fig. 2(a), let $t_k (k = 1,2,3\cdots)$ be the sampling time instant at which new optimal control decisions should be executed to control vehicles in the platoon, T_P be the prediction horizon for which the optimal control decisions are determined, and Δt ($\Delta t \leq T_P$) be the roll period for which these decisions are implemented. Such a rolling horizon framework enables the practical implementation of the control strategy by trading off (solution) computational time with solution accuracy by limiting the prediction horizon size while being responsive to unfolding traffic conditions. Thereby, for a sampling time instant t_k, the new optimal control decisions are calculated for the prediction horizon $[t_k, t_k + T_P]$, but only implemented for the roll period $[t_k, t_k + \Delta t]$ by the following vehicles in the platoon to control their behavior. Then, at the next sampling time instant t_{k+1} (where $t_{k+1} = t_k + \Delta t$), the procedure is repeated to determine and implement the optimal control decisions for all following CAVs in the platoon for roll period $[t_{k+1}, t_{k+1} + \Delta t]$. This procedure is repeated until the platoon dissipates.

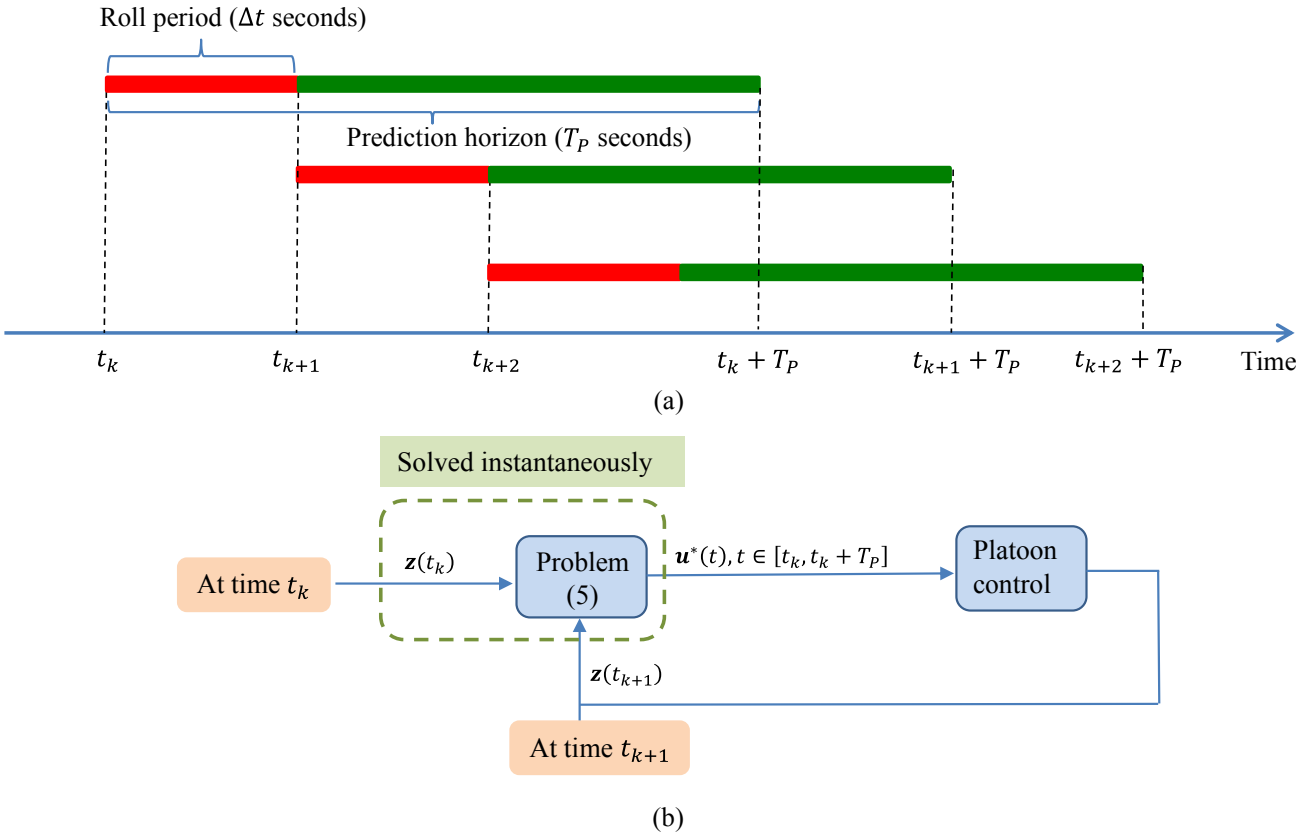

Fig.2. The idealized MPC strategy: (a) Implementation framework, and (b) Computational procedure.

Next, the idealized MPC strategy to determine the optimal control decisions and its computational

procedure are exposited. Let $\mathbf{z}(t) = [\mathbf{x}(t)^T, \quad \mathbf{y}(t)^T]^T$. Following Wang et al. (2014b) and Zhou et al. (2017), at each sampling time instant t_k, $\forall k = 0,1,2\cdots$, the optimal control decisions of all of the following vehicles in the platoon can be obtained by solving the following optimal control problem:

$$\min_{\boldsymbol{u}} \int_0^{T_P} \frac{1}{2} e^{-\beta t} L(\boldsymbol{z}(t), \boldsymbol{u}(t))\, dt + \frac{1}{2} e^{-\beta T_P} \phi(\mathbf{z}(T_P)) \tag{5a}$$

$$\dot{\mathbf{z}}(t) = \boldsymbol{A} \cdot \mathbf{z}(t) + \boldsymbol{B} \cdot \boldsymbol{u}(t) \tag{5b}$$

$$s_i(t) = x_i(t) + r^* \cdot \left(v_0(0) + \sum\nolimits_{j=1}^{i} y_j(t) \right) + s_f \geq \mathrm{s}_{min}; i = 1,2,\cdots,n \tag{5c}$$

$$0 \leq v_i(t) \leq v_{max}; i = 1,2,\cdots,n \tag{5d}$$

$$u_{min} \leq u_i \leq u_{max}; \; i = 1,2,\cdots,n \tag{5e}$$

$$\mathbf{z}(0) = [\mathbf{x}_0^T \quad \mathbf{y}_0^T]^T \tag{5f}$$

where

$$L(\boldsymbol{z}(t), \boldsymbol{u}(t)) = \mathbf{z}(t)^T \begin{bmatrix} \boldsymbol{R}_1 & \\ & \boldsymbol{R}_2 \end{bmatrix} \mathbf{z}(t) + \boldsymbol{u}(t)^T \boldsymbol{R}_3 \boldsymbol{u}(t) \tag{5g}$$

$$\phi(\mathbf{z}(T_P)) = \mathbf{z}(T_P)^T \begin{bmatrix} \boldsymbol{R}_4 & \\ & \boldsymbol{R}_5 \end{bmatrix} \mathbf{z}(T_P) \tag{5h}$$

In problem (5), for expository convenience, we consider a generic prediction horizon and ignore the sampling time instant t_k. So, $t \in [0, T_P]$ without loss of generality in (5). Here, $\boldsymbol{R}_1, \boldsymbol{R}_2, \boldsymbol{R}_3$ $\boldsymbol{R}_4$, and $\boldsymbol{R}_5$ are weight matrices; $\boldsymbol{R}_1, \boldsymbol{R}_2,$ $\boldsymbol{R}_4$, and $\boldsymbol{R}_5$ are symmetric positive definite matrices; and $\boldsymbol{R}_3$ is a positive definite diagonal matrix (Zhou et al., 2017). $L(\boldsymbol{z}(t), \boldsymbol{a}(t))$ is the running cost which is the cost incurred during an infinitesimal period (Wang et al. 2014b). It consists of two terms. The first term $\mathbf{z}(t)^T \begin{bmatrix} \boldsymbol{R}_1 & \\ & \boldsymbol{R}_2 \end{bmatrix} \mathbf{z}(t)$ seeks to minimize the position errors and the relative speed of all adjacent vehicle pairs. The second component (i.e., $\boldsymbol{u}(t)^T \boldsymbol{R}_3 \boldsymbol{u}(t)$) is to maximize comfort by reducing hard braking and acceleration. $e^{-\beta t}$ is a term to weight the running cost at different times and β is the discount coefficient. This term provides higher weight for the running cost for the near-term future than for the longer-term future as the uncertainty in running cost increases with time (Wang et al., 2014b). $\phi(\mathbf{z}(T_P))$ is the terminal cost which is used to penalize the value of objective function if the values of the state variables at the end of the prediction horizon deviate from the equilibrium point (i.e., 0). Eq. (5b) describes the dynamics of the state variables (i.e., position errors and relative speeds of all adjacent vehicle pairs in the platoon). Eq. (5c) is a safety constraint to ensure that the spacing between two consecutive CAVs in the platoon is always larger than a positive lower bound s_{min}, $\mathrm{s}_{min} > 0$. Eq. (5d) specifies that the range of the speed of each vehicle in the platoon. v_{max} is the speed limit of the road. Eq. (5e) specifies the upper bound (u_{max}) and lower bound (u_{min}) of the acceleration. These inequality constraints are extensively used in the literature for designing effective control method for CAV platoons (see e.g., Wang et al., 2018; Lu et al., 2019). Eq. (5f) specifies the initial inputs for the state variables. Hence, for example, for any sampling time instant t_k, $\mathbf{x}_k = [x_1(t_k), x_2(t_k), \cdots, x_n(t_k)]$ and $\mathbf{y}_k = [y_1(t_k), y_2(t_k), \cdots, y_n(t_k)]$ are values of $\mathbf{x}_0^T$ and $\mathbf{y}_0^T$, respectively.

There are primarily two differences between optimal control problem (5) and the ones developed by Wang et al. (2014b) and Zhou et al. (2017). First, a term $e^{-\beta t}$ is added to the objective function to weight

the running costs at different times. Second, a terminal cost $\phi(\mathbf{z}(T_P))$ is added to penalize the objective function if the state variables deviate from the equilibrium point 0 at the end of the prediction horizon. These two terms will be useful to analyze the stability of the idealized MPC strategy. In addition, for convenience of stability analysis, the weight matrices $\boldsymbol{R}_i(i = 1,2,4,5)$ are assumed to have the following forms:

$$\boldsymbol{R}_1 = \boldsymbol{\Lambda}^T \boldsymbol{D}_a \boldsymbol{\Lambda}, \boldsymbol{R}_2 = \boldsymbol{\Lambda}^T \boldsymbol{D}_b \boldsymbol{\Lambda}, \boldsymbol{R}_4 = \boldsymbol{\Lambda}^T \boldsymbol{D}_c \boldsymbol{\Lambda}, \text{ and } \boldsymbol{R}_5 = \boldsymbol{\Lambda}^T \boldsymbol{D}_e \boldsymbol{\Lambda} \quad (6)$$

where $\boldsymbol{\Lambda}$ is an orthogonal matrix, $\boldsymbol{\Lambda}^T \boldsymbol{\Lambda} = \boldsymbol{\Lambda} \boldsymbol{\Lambda}^T = \boldsymbol{E}_n$, and $\boldsymbol{D}_a$, $\boldsymbol{D}_b$, $\boldsymbol{D}_c$ and $\boldsymbol{D}_e$ are positive definite diagonal matrices. The inputs of these weight matrices will be determined by the stability analysis in Section 5. Eq. (6) shows that if $\boldsymbol{\Lambda} = \boldsymbol{E}_n$, then $\boldsymbol{R}_1$, $\boldsymbol{R}_2$, $\boldsymbol{R}_4$, and $\boldsymbol{R}_5$ are positive definite diagonal matrices.

Let $\mathbf{z}(t_k)$ be the actual values of the state variables at the sampling time instant $t_k, (k = 1,2, \cdots)$, $\mathbf{z}(t_k) = [\mathbf{x}_k^T \quad \mathbf{y}_k^T]^T$. The computational procedure of the idealized MPC strategy is summarized in Fig. 2(b). At each sampling time instant $t_k(k = 1,2, \cdots)$, the leading vehicle obtains the value of $\mathbf{z}(t_k)$ through V2V communications. It solves the optimal control problem (5) to determine the optimal control decisions (i.e.,$\boldsymbol{u}^*(t)$) during the prediction horizon $[t_k, t_k + T_P]$ by inputting the value of $\mathbf{z}(t_k)$ into Eq. (5e). The optimal control decisions are sent by the leading vehicle to the following vehicles to control their behaviors only for the roll period $[t_k, t_k + \Delta t]$, (i.e., $[t_k, t_{k+1}]$). Then, at the sampling time instant t_{k+1}, the optimal control problem (5) is solved again to obtain the optimal control decisions $\boldsymbol{u}^*(t)$ for the prediction horizon $[t_{k+1}, t_{k+1} + T_P]$, and is implemented to control the CAV platoon for the roll period $[t_{k+1}, t_{k+1} + \Delta t]$. These steps are repeated at each sampling time instant.

As can be noted, the idealized MPC strategy computes the optimal control decisions by solving optimal control problem (5) at each sampling time instant and implements it to control the CAVs for the roll period starting at that instant. To achieve this, it is assumed that the leading vehicle can solve the optimal control problem (5) of the idealized MPC strategy instantaneously at each sampling time instant t_k. However, in practice, the computational time for solving optimal control problem (5) increases with platoon size and prediction horizon size. It can cause significant delays in executing the control decisions, which can deteriorate the performance and even lead to vehicle collisions. Thereby, while the idealized MPC strategy can coordinate the behavior of the following vehicles in the platoon to maneuver them efficiently and safely, it cannot be deployed to control the CAV platoon in real-time.

2.2 DMPC approach framework

The leading vehicle of a CAV platoon needs to respond to the dynamics of the vehicles downstream of it. Thereby, its behavior is not known in advance. However, the behavior of all following vehicles in the platoon for each roll period can be estimated at the corresponding sampling time instant through the known optimal control decisions of the previous roll period (i.e., $\boldsymbol{u}^*(t)$, $t \in [t_{k-1}, t_{k-1} + \Delta t]$). To account for this difference, we divide $\mathbf{z}(t)$ into two parts, $\boldsymbol{z}_1(t)$ and $\boldsymbol{z}_2(t)$. We denote the vector of position error and speed difference of vehicle 1 from that of the leading vehicle 0 as $\boldsymbol{z}_1(t) = [x_1(t), y_1(t)]^T$, and the vector of state variables for the other following vehicles as $\boldsymbol{z}_2(t) = [x_2(t), x_3(t), \cdots, x_n(t), y_2(t), y_3(t), \cdots, y_n(t)]^T$. At each sampling time instant t_k, the value of $\boldsymbol{z}_1(t_k)$ cannot be computed in advance due to the unknown position and speed of the leading vehicle at that instant. However, $\mathbf{z}_2(t_k)$ can be estimated in advance at a short time before the sampling time instant t_k.

We propose the DMPC approach to address the strong assumption of the idealized MPC strategy

that the optimal control problem (5) can be solved instantaneously. The implementation framework for the DMPC approach is shown in Fig. 3(a). Unlike the idealized MPC strategy, the DMPC approach reserves a sufficient amount of time, labeled reserved time (denoted as τ_1), before each sampling time instant t_k $(k = 1,2,\cdots)$ to solve the optimal control problem (5) so that the optimal control decisions are available at t_k for the corresponding roll period. It is important to note that the roll period Δt should be larger than τ_1 to enable the real-time implementation of the DMPC approach.

The DMPC computational procedure is illustrated in Fig. 3(b). The DMPC approach starts to solve the optimal control problem at time $t_k - \tau_1$ to predict the values of all state variables at time t_k (i.e., $\mathbf{z}(t_k)$). As stated in the assumptions, the leading vehicle can obtain the actual states of all following vehicles at time instant $t_k - \tau_1$ through V2V communications. Also, as discussed earlier in this section, it knows the control decisions of all following vehicles in the time period $[t_k - \tau_1, t_k]$ as they are determined at the beginning of the previous roll period. The DMPC approach leverages these two sets of inputs to predict $\mathbf{z}_2(t_k)$ with low error. This is because in the context of the CAV platooning application, τ_1 is much smaller than the roll period, in the order of a fraction of a second. Hence, as the actual states are available close to t_k, and prior control decisions are known, we assume that the error in estimating $\mathbf{z}_2(t_k)$ is negligible.

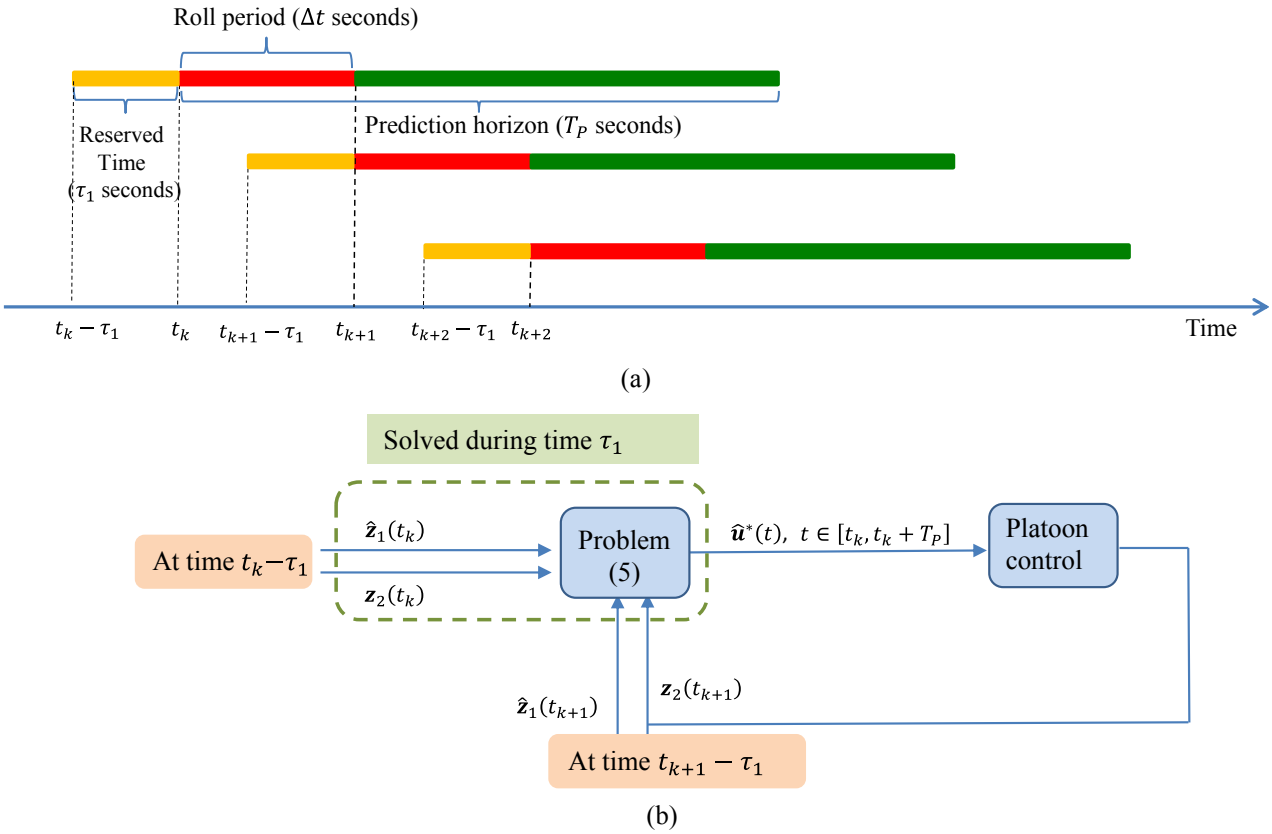

Fig. 3. The DMPC approach: (a) Implementation framework, and (b) Computational procedure.

As discussed earlier, the leading vehicle's behavior is not known in advance. Thereby, $\mathbf{z}_1(t_k)$ cannot be estimated with low error unlike $\mathbf{z}_2(t_k)$. Hence, the value of $\mathbf{z}_1(t_k)$ needs to be predicted at time instant $t_k - \tau_1$. To do so, the leading vehicle's behavior at t_k needs to be predicted at $t_k - \tau_1$. As τ_1 is much smaller than the roll period, we assume the acceleration of the leading vehicle 0 during the small

time interval $[t_k - \tau_1, t_k]$ remains the same as at time instant $t_k - \tau_1$. Then,

$$\hat{v}_0(t_k) = v_0(t_k - \tau_1) + u_0(t_k - \tau_1) \cdot \tau_1 \tag{7a}$$

$$\hat{d}_0(t_k) = d_0(t_k - \tau_1) + v_0(t_k - \tau_1) \cdot \tau_1 + 0.5 \cdot u_0(t_k - \tau_1) \cdot (\tau_1)^2 \tag{7b}$$

where $\hat{v}_0(t_k)$ and $\hat{d}_0(t_k)$ are the predicted speed and predicted position of the leading vehicle at time instant t_k, respectively. Here, $v_0(t_k - \tau_1)$, $d_0(t_k - \tau_1)$ and $u_0(t_k - \tau_1)$ are the actual speed, position and acceleration of the leading vehicle at $t_k - \tau_1$, respectively, that are detected through onboard sensors. The position error and relative speed of vehicle 1 from that of the leading vehicle 0 at time instant t_k can then be predicted as:

$$\hat{x}_1(t_k) = \hat{d}_0(t_k) - d_1(t_k) - r^* \cdot v_1(t_k) - s_f \tag{8a}$$

$$\hat{y}_1(t_k) = v_1(t_k) - \hat{v}_0(t_k) \tag{8b}$$

where $\hat{x}_1(t_k)$ and $\hat{y}_1(t_k)$ are the predicted position error and speed difference of vehicle 1 with respect to the leading vehicle 0 at time t_k, respectively. Note that the speed and position of vehicle 1 at time instant $t_k - \tau_1$ are detected through the onboard sensors, and the corresponding control decision $u_1(t)$, $t \in [t_k - \tau_1, t_k]$ is known. Then, $d_1(t_k)$ and $v_1(t_k)$ can be computed as:

$$v_1(t_k) = v_1(t_k - \tau_1) + \int_{t_k - \tau_1}^{t_k} u_1(t)\, dt \tag{9a}$$

$$\begin{aligned} d_1(t_k) &= d_1(t_k - \tau_1) + \int_{t_k - \tau_1}^{t_k} v_1(t)\, dt \\ &= d_1(t_k - \tau_1) + \int_{t_k - \tau_1}^{t_k} \left[v_1(t_k - \tau_1) + \left(\int_{t_k - \tau_1}^{t} u_1(\varsigma) d\varsigma \right) \right] dt \end{aligned} \tag{9b}$$

Note that the predicted value $\hat{\mathbf{z}}_1(t_k)$ ($\hat{\mathbf{z}}_1(t_k) = [\hat{x}_1(t_k), \hat{y}_1(t_k)]$) is different from the actual value $\boldsymbol{z}_1(t_k)$ due to the error in predicting the leading vehicle's position and speed. Thereby, the estimated control decisions of the DMPC approach (i.e., $\hat{\boldsymbol{u}}(t)$) are different from the optimal control decisions computed by the idealized MPC strategy (i.e., $\boldsymbol{u}^*(t)$). In the numerical experiments, we will show that the estimated control decisions of the DMPC approach will deviate significantly from those of the idealized MPC strategy when the error in predicting $\boldsymbol{z}_1(t_k)$ is large. This will deteriorate the efficiency of the CAV platoon and can cause vehicular collisions.

It should be noted that other models can also be used to predict the leading vehicle's state. However, prediction error exists for all models as the leading vehicle's behavior is unknown, which may impact the control performance of the DMPC approach.

2.3 DMPC-FOA approach framework

The DMPC approach circumvents the strong assumption of the idealized MPC strategy at the cost that the estimated control decisions may deviate significantly from those of the idealized MPC strategy due to the error in predicting $\boldsymbol{z}_1(t_k)$. To address this problem, we propose the DMPC-FOA approach which simultaneously addresses the control delay issue of the idealized MPC strategy while more accurately characterizing the optimal control decisions.

Let τ_2 be the reserved time for computing the optimal control decisions for the DMPC-FOA

approach. Also, let $\tilde{\boldsymbol{z}}_1(t_k) = [\tilde{x}_1(t_k) \quad \tilde{y}_1(t_k)]$ be the predicted value of $\boldsymbol{z}_1(t_k)$ for the DMPC-FOA approach at time instant $t_k - \tau_2$ by replacing τ_1 with τ_2 in Eqs. (7) and (8). Here, $\tilde{x}_1(t_k)$ and $\tilde{y}_1(t_k)$ are the predicted position error and speed difference of vehicle 1 with respect to the leading vehicle at time instant t_k, respectively. Similar to the DMPC approach, we assume the error in estimating $\mathbf{z}_2(t_k)$ is negligible as the actual states (i.e., $\mathbf{z}_2(t_k - \tau_2)$) are available close to t_k, and prior control decisions are known.

Denote $\boldsymbol{\gamma}(t)$ as the vector of costate variables associated with the state equations (5b). The costate variables indicate the change in the objective function value for a unit change in the corresponding state variable at the optimal state (Gaimon, 2002). The computational procedure for the DMPC-FOA approach is illustrated in Fig. 4, where $\tilde{\boldsymbol{z}}^*(t)$ and $\tilde{\boldsymbol{\gamma}}^*(t), t \in [t_k, t_k + T_P]$ are the solutions for the state and costate variables obtained by solving optimal control problem (5) with initial inputs $[\tilde{\boldsymbol{z}}_1(t_k), \boldsymbol{z}_2(t_k)]$). The optimal control decisions for the idealized MPC strategy, $\varphi\big(\boldsymbol{z}^*(t), \boldsymbol{\gamma}^*(t)\big)$ (denoted as $\boldsymbol{u}^*(t)$), are analytically derived in Section 3 (see Eq. (23)) which discusses the solution algorithm. Then, $\boldsymbol{u}^*(t), t \in [t_k, t_k + T_P]$ can be approximated by $\varphi\big(\tilde{\boldsymbol{z}}^*(t), \tilde{\boldsymbol{\gamma}}^*(t)\big)$ (denoted as $\tilde{\boldsymbol{u}}^*(t)$). Note that the difference between $[\tilde{\boldsymbol{z}}^*(t), \tilde{\boldsymbol{\gamma}}^*(t)]$ and $[\boldsymbol{z}^*(t), \boldsymbol{\gamma}^*(t)]$ significantly impacts the accuracy of the estimated control decisions $\tilde{\boldsymbol{u}}^*(t)$. To reduce the difference between $\tilde{\boldsymbol{u}}^*(t)$ and $\boldsymbol{u}^*(t), t \in [t_k, t_k + T_P]$, sensitivity analysis of the optimal control problem (5) is performed to determine the derivatives of $\partial\tilde{\boldsymbol{z}}^*(t)/\partial\,\tilde{\boldsymbol{z}}_1(t_k)$ (i.e., $\left[\frac{\partial\,\tilde{\boldsymbol{z}}^*(t)}{\partial\tilde{x}_1(t_k)}, \frac{\partial\,\tilde{\boldsymbol{z}}^*(t)}{\partial\tilde{y}_1(t_k)}\right]$) and $\partial\tilde{\boldsymbol{\gamma}}^*(t)/\partial\,\tilde{\boldsymbol{z}}_1(t_k)$ (i.e., $\left[\frac{\partial\,\tilde{\boldsymbol{\gamma}}^*(t)}{\partial\tilde{x}_1(t_k)}, \frac{\partial\,\tilde{\boldsymbol{\gamma}}^*(t)}{\partial\tilde{y}_1(t_k)}\right]$). These two terms can quantitatively measure the changes in the optimal solutions for $\tilde{\boldsymbol{z}}^*(t)$ and $\tilde{\boldsymbol{\gamma}}^*(t)$ for a unit increase in $\tilde{\boldsymbol{z}}_1(t_k)$. Thereby, at sampling time instant t_k when the actual value of $x_1(t_k)$ and $y_1(t_k)$ are detected through onboard sensors, the first-order Taylor's approximation is applied to better estimate the solutions of $\boldsymbol{z}^*(t)$ and $\boldsymbol{\gamma}^*(t)$, as follows:

$$\bar{\boldsymbol{z}}^*(t) = \tilde{\boldsymbol{z}}^*(t) + \frac{\partial\,\tilde{\boldsymbol{z}}^*(t)}{\partial\tilde{x}_1(t_k)}\big(x_1(t_k) - \tilde{x}_1(t_k)\big) + \frac{\partial\,\tilde{\boldsymbol{z}}^*(t)}{\partial\tilde{y}_1(t_k)}\Big(y_1(t_k) - \tilde{y}_1(t_k)\Big), t \in [t_k, t_k + T_P] \quad (10a)$$

$$\bar{\boldsymbol{\gamma}}^*(t) = \tilde{\boldsymbol{\gamma}}^*(t) + \frac{\partial\,\tilde{\boldsymbol{\gamma}}^*(t)}{\partial\tilde{x}_1(t_k)}\big(x_1(t_k) - \tilde{x}_1(t_k)\big) + \frac{\partial\,\tilde{\boldsymbol{\gamma}}^*(t)}{\partial\tilde{y}_1(t_k)}\Big(y_1(t_k) - \tilde{y}_1(t_k)\Big), t \in [t_k, t_k + T_P] \quad (10b)$$

where $\bar{\boldsymbol{z}}^*(t)$ and $\bar{\boldsymbol{\gamma}}^*(t)$ are the values of $\boldsymbol{z}^*(t)$ and $\boldsymbol{\gamma}^*(t)$ estimated by the DMPC-FOA approach, respectively.

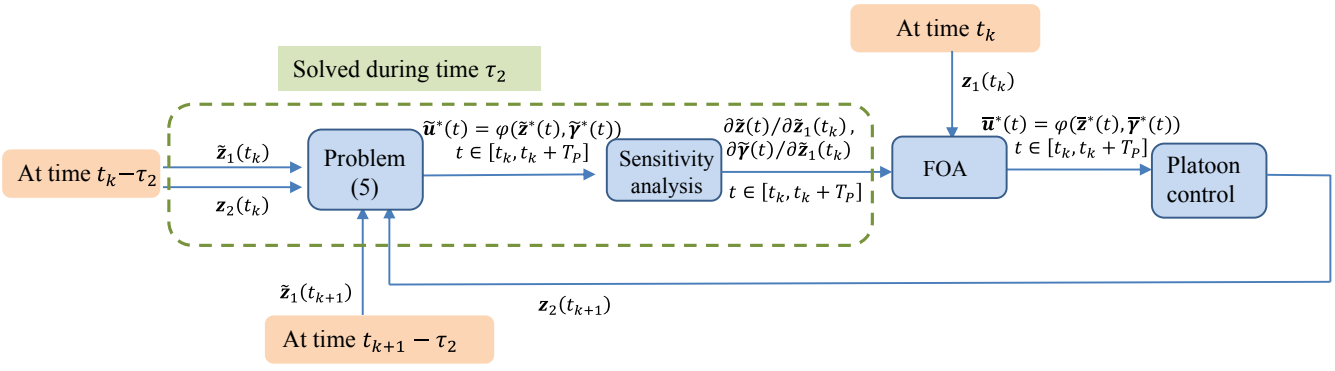

Fig. 4. Computational procedure of the DMPC-FOA approach.

When compared to $[\tilde{\boldsymbol{z}}^*(t), \tilde{\boldsymbol{\gamma}}^*(t)]$, $[\bar{\boldsymbol{z}}^*(t), \bar{\boldsymbol{\gamma}}^*(t)]$ are closer to $[\boldsymbol{z}^*(t), \boldsymbol{\gamma}^*(t)]$. Thereby, in Fig. 4,

the estimated control decisions $\overline{\boldsymbol{u}}^*(t) = \varphi\big(\overline{\boldsymbol{z}}^*(t), \overline{\boldsymbol{\gamma}}^*(t)\big)$ are closer to $\boldsymbol{u}^*(t)$ compared to $\widetilde{\boldsymbol{u}}^*(t), t \in [t_k, t_k + T_P]$. It is important to note here that Eq. (10) can be calculated instantaneously if the derivatives are obtained before the sampling time instant t_k. In addition, $\varphi\big(\overline{\boldsymbol{z}}^*(t), \overline{\boldsymbol{\gamma}}^*(t)\big)$ can also be calculated instantaneously due to the closed-form formulation (Eq. (23)). Thereby, the DMPC-FOA approach can be applied for real-time control of the CAV platoon with no control delay.

As can be noted, before each sampling time instant t_k, the DMPC-FOA approach needs to solve the optimal control problem (5) and conduct sensitivity analysis. Hence, the reserved time $\tau_2 \geq \tau_1$. Nevertheless, we will show using numerical examples that the gap between $\overline{\boldsymbol{u}}^*(t)$ and $\boldsymbol{u}^*(t)$ is negligible even for large prediction errors of $\boldsymbol{z}_1(t_k)$ at every sampling time instant t_k.

3. Solution algorithm for optimal control problem (5)

To solve optimal control problem (5), a two-point boundary value problem is developed in this section based on the necessary conditions for optimality, the solution of which determines the optimal control decisions for all following CAVs. The two-point boundary value problem can be solved efficiently using methods such as the shooting method (Keller, 1976), method of steepest descent (Kirk, 2012), and iterative algorithm (Wang et al., 2014a).

Optimal control problem (5) contains control constraints (Eq. (5d)) and pure state variable inequality constraints (5c). The presence of pure state variable inequality constraints increases the difficulty in designing an effective solution algorithm as these constraints depend on the control history. To address this problem, optimal control problem (5) is converted to an equivalent optimal control problem without pure state variable inequality constraints. To do so, we define a new variable z_N that has the following functional relationship

$$\dot{z}_N(t) = \sum_{i=1}^{n} \big(z_{N,1}^i + z_{N,2}^i + z_{N,3}^i\big) \tag{11}$$

where

$$z_{N,1}^i = [s_i(t) - \mathrm{s}_{min}]^2 I(s_i(t) - \mathrm{s}_{min})$$
$$z_{N,2}^i = [v_{max} - v_i(t)]^2 I\big(v_{max} - v_i(t)\big)$$
$$z_{N,3}^i = v_i(t) I\big(v_i(t)\big)$$
$$I(s_i(t) - \mathrm{s}_{min}) = \begin{cases} 0, if \;\; s_i(t) - \mathrm{s}_{min} \geq 0 \\ 1, \quad otherwise \end{cases}$$
$$I\big(v_{max} - v_i(t)\big) = \begin{cases} 0, if \;\; v_{max} - v_i(t) \geq 0 \\ 1, \quad otherwise \end{cases}$$
$$I\big(v_i(t)\big) = \begin{cases} 0, if \;\; v_i(t) \geq 0 \\ 1, otherwise \end{cases}$$

Proposition 1: If $z_N(0) = z_N(T_P) = 0$, then $s_i(t) \geq \mathrm{s}_{min}$ and $0 \leq v_i(t) \leq v_{max}; i = 1,2,\cdots,n$ for $t \in [0, T_P]$.

Proof: According to Eq. (11), $z_N(t)$ is a continuous function of time t and $\dot{z}_N(t) \geq 0$. Thereby, $z_N(t)$ is a non-decreasing function of time t. Since $z_N(0) = z_N(T_P) = 0$, this implies that $\dot{z}_N(t) \equiv 0$ for $t \in [0, T_P]$ (otherwise, $z_N(T_P) = \int_0^{T_P} \dot{z}_N(t)\, dt + z_N(0) = \int_0^{T_P} \dot{z}_N(t)\, dt > 0$). According to Eq. (11),

$\dot{z}_N(t) \equiv 0$ if and only if $s_i(t) \geq s_{min}$ and $v_i(t) \leq v_{max}; i = 1,2,\cdots,n$ for $t \in [0, T_P]$. This completes the proof.

According to Proposition 1, the optimal control problem (5) can be rewritten as the following equivalent problem:

$$\min_{\boldsymbol{u}} \int_0^{T_P} \frac{1}{2} e^{-\beta t} [\mathbf{z}(t)^T \boldsymbol{Q}_1 \mathbf{z}(t) + \boldsymbol{u}(t)^T \boldsymbol{R}_3 \boldsymbol{u}(t)]\, dt + \frac{1}{2} e^{-\beta T_P} \mathbf{z}(T_P)^T \boldsymbol{Q}_2 \mathbf{z}(T_P) \tag{12a}$$

$$\dot{\mathbf{z}}(t) = \boldsymbol{A} \cdot \mathbf{z}(t) + \boldsymbol{B} \cdot \boldsymbol{u}(t) \tag{12b}$$

$$\dot{z}_N(t) = \sum_{i=1}^{n} \left(z_{N,1}^i + z_{N,2}^i + z_{N,3}^i \right) \tag{12c}$$

$$u_{min} \leq u_i \leq u_{max}; i = 1,2,\cdots n \tag{12d}$$

$$\mathbf{z}(0) = [\mathbf{x}_0^T \quad \mathbf{y}_0^T]^T; z_N(0) = z_N(T_P) = 0 \tag{12e}$$

where

$$\boldsymbol{Q}_1 = \begin{bmatrix} \boldsymbol{R}_1 & \\ & \boldsymbol{R}_2 \end{bmatrix}; \boldsymbol{Q}_2 = \begin{bmatrix} \boldsymbol{R}_4 & \\ & \boldsymbol{R}_5 \end{bmatrix}$$

To develop a two-point boundary value problem based on the necessary conditions for optimality of optimal control problem (5), the terminal condition $z_N(T_P) = 0$ is removed from Eq. (12e). To ensure $z_N(T_P) \to 0$, similar to the study of Naidu (2003), the term $\mathrm{M} \cdot \left(z_N(T_P)\right)^2$ is added to the objective function, where M is a sufficiently large number. If $z_N(T_P) \neq 0$, the objective function is penalized. The optimal control problem (12) can then be re-written as:

$$\min_{\boldsymbol{u}} \int_0^{T_P} \frac{1}{2} e^{-\beta t} [\mathbf{z}(t)^T \boldsymbol{Q}_1 \mathbf{z}(t) + \boldsymbol{u}(t)^T \boldsymbol{R}_3 \boldsymbol{u}(t)]\, dt + \frac{1}{2} e^{-\beta T_P} \mathbf{z}(T_P)^T \boldsymbol{Q}_2 \mathbf{z}(T_P) + \mathrm{M} \cdot \left(z(T_P)\right)^2 \tag{13a}$$

$$\dot{\mathbf{z}}(t) = \boldsymbol{A} \cdot \mathbf{z}(t) + \boldsymbol{B} \cdot \boldsymbol{u}(t) \tag{13b}$$

$$\dot{z}_N(t) = \sum_{i=1}^{n} \left(z_{N,1}^i + z_{N,2}^i + z_{N,3}^i \right) \tag{13c}$$

$$u_{min} \leq u_i \leq u_{max}; i = 1,2,\cdots n \tag{13d}$$

$$\mathbf{z}(0) = [\mathbf{x}_0^T \quad \mathbf{y}_0^T]^T; z_N(0) = 0 \tag{13e}$$

Optimal control problem (13) is equivalent to problem (5). It contains only control constraints. Define the vector of functions $\mathbf{f}_1(\boldsymbol{z}(t), \boldsymbol{u}(t))$ and the function $\mathrm{f}_2(\boldsymbol{z}(t), \boldsymbol{u}(t))$ as follows:

$$\dot{\mathbf{z}}(t) = \begin{bmatrix} \dot{\mathbf{x}}(t) \\ \dot{\mathbf{y}}(t) \end{bmatrix} = \mathbf{f}_1(\boldsymbol{z}(t), \boldsymbol{u}(t)) = \boldsymbol{A} \cdot \mathbf{z}(t) + \boldsymbol{B} \cdot \boldsymbol{u}(t) \tag{14a}$$

$$\dot{z}_N(t) = \mathrm{f}_2\left(\boldsymbol{z}(t), \boldsymbol{u}(t)\right) = \sum_{i=1}^{n} \left(z_{N,1}^i + z_{N,2}^i + z_{N,3}^i \right) \tag{14b}$$

Then, the Hamiltonian function for optimal control problem (13) is written as:

$$\boldsymbol{H}(\boldsymbol{z}(t), \boldsymbol{\lambda}_A(t), \boldsymbol{u}(t)) = e^{-\beta t} L\left(\boldsymbol{z}(t), \boldsymbol{u}(t)\right) + \boldsymbol{\lambda}(t)^T \cdot \mathbf{f}_1\left(\boldsymbol{z}(t), \boldsymbol{u}(t)\right) + \lambda_N(t) \cdot \mathrm{f}_2(\boldsymbol{z}(t), \boldsymbol{u}(t)). \tag{15}$$

where $\boldsymbol{\lambda}(t) = [\lambda_1(t) \quad \cdots \quad \lambda_{2n}(t)]^T$ and $\lambda_N(t)$ are the costate variables associated with $\mathbf{f}_1\left(\boldsymbol{z}(t), \boldsymbol{u}(t)\right)$ and $\mathrm{f}_2(\boldsymbol{z}(t), \boldsymbol{u}(t))$, respectively. Let $\boldsymbol{\lambda}_A(t) = [\boldsymbol{\lambda}(t)^T, \lambda_N(t)]^T$, and $\boldsymbol{z}_A(t) = [\boldsymbol{z}(t)^T, z_N(t)]^T$. According to Pontryagin's minimum principle, the necessary conditions for $\boldsymbol{u}^*(t)$ to be an optimal solution for

problem (13) are

$$\dot{\boldsymbol{\lambda}}_A(t) = -\left(\frac{\partial \boldsymbol{H}}{\partial \boldsymbol{z}_A(t)}\right) \tag{16a}$$

$$\begin{bmatrix} \dot{\mathbf{z}}(t) \\ \dot{z}_N(t) \end{bmatrix} = \begin{bmatrix} \mathbf{f}_1(\boldsymbol{z}(t), \boldsymbol{u}(t)) \\ \mathrm{f}_2(\boldsymbol{z}(t), \boldsymbol{u}(t)) \end{bmatrix} \tag{16b}$$

with the initial conditions given in Eq. (13e) and the terminal conditions as:

$$\begin{aligned} \boldsymbol{\lambda}(T_P) &= \partial\left(\frac{1}{2} e^{-\beta T_P} \mathbf{z}(t)^T \boldsymbol{Q}_2 \mathbf{z}(t)\right) \Big/ \partial \mathbf{z}(t)\Big|_{t=T_P} \\ &= e^{-\beta T_P} \cdot \boldsymbol{Q}_2 \cdot \mathbf{z}(T_P); \end{aligned} \tag{16c}$$

$$\begin{aligned} \lambda_N(T_P) &= \partial(\mathrm{M} \cdot z_N(t)^2)/\partial z_N(t)|_{t=T_P} \\ &= 2\,\mathrm{M} \cdot z_N(T_P). \end{aligned} \tag{16d}$$

In addition, the optimal state trajectory $\boldsymbol{z}^*(t)$, the optimal costate trajectory $\boldsymbol{\lambda}_A^*(t)$ and the optimal control decisions $\boldsymbol{u}^*(t)$ should satisfy

$$\boldsymbol{H}(\boldsymbol{z}^*(t), \boldsymbol{\lambda}_A^*(t), \boldsymbol{u}^*(t)) \leq \boldsymbol{H}\big(\boldsymbol{z}^*(t), \boldsymbol{\lambda}_A^*(t), \boldsymbol{u}(t)\big);\ \ \boldsymbol{u}(t), \boldsymbol{u}^*(t) \in \boldsymbol{\mathcal{U}} \tag{16e}$$

where $\boldsymbol{\mathcal{U}} = \{\boldsymbol{u} | u_{min} \leq u_i \leq u_{max};\ i = 1,2,\cdots n\}$. To convert these necessary conditions for optimality into a two-point boundary value problem, we define the current-value Hamiltonian function as follows:

$$\boldsymbol{H_c} = e^{\beta t}\boldsymbol{H} = L(\boldsymbol{z}(t), \boldsymbol{u}(t)) + \boldsymbol{\gamma}(t)^T \mathbf{f}_1(\boldsymbol{z}(t), \boldsymbol{u}(t)) + \gamma_N(t)\mathrm{f}_2(\boldsymbol{z}(t), \boldsymbol{u}(t)). \tag{17}$$

where $\boldsymbol{\gamma}(t) = \boldsymbol{\lambda}(t)e^{\beta t}, \gamma_N = \lambda_N(t)e^{\beta t}$ are the costate variables for the current-value Hamiltonian function. Since the discount factor $e^{-\beta t}$ does not depend on the control variables, the optimal control $\boldsymbol{u}^*$ that minimizes the Hamiltonian function $\boldsymbol{H}$ must also minimize the current-value Hamiltonian function (Eq. (17)). Let $\boldsymbol{\gamma}_A = [\boldsymbol{\gamma}(t)^T, \gamma_N(t)]^T$**.** Then,

$$\dot{\boldsymbol{\lambda}}_A(t) = -\beta e^{-\beta t}\boldsymbol{\gamma}_A(t) + e^{-\beta t}\dot{\boldsymbol{\gamma}}_A(t). \tag{18a}$$

$$\frac{\partial \boldsymbol{H}}{\partial \boldsymbol{z}_A(t)} = \frac{\partial \boldsymbol{H}_c}{\partial \boldsymbol{z}_A(t)} e^{-\beta \cdot t} \tag{18b}$$

Eqs. 18(a) and 18(b) imply

$$\dot{\boldsymbol{\gamma}}_A(t) = \dot{\boldsymbol{\lambda}}_A(t) + \beta \boldsymbol{\gamma_A}(t) \tag{19}$$

Thereby,

$$\begin{aligned} \dot{\boldsymbol{\gamma}}(t) &= -\frac{\partial \boldsymbol{H}_c}{\partial \boldsymbol{z}} + \beta\boldsymbol{\gamma}(t) \\ &= -\frac{\partial\, \mathbf{f}_1(\boldsymbol{z}, \boldsymbol{u})}{\partial \boldsymbol{z}}\boldsymbol{\gamma}(t) - \frac{\partial \mathrm{f}_2(\boldsymbol{z}, \boldsymbol{u})}{\partial \boldsymbol{z}}\gamma_N(t) - \frac{\partial\, L(\boldsymbol{z}, \boldsymbol{u})}{\partial \boldsymbol{z}} + \beta\boldsymbol{\gamma}(t) \\ &= -\boldsymbol{A} \cdot \boldsymbol{\gamma}(t) - \begin{bmatrix} \boldsymbol{C}_x \\ \boldsymbol{C}_y \end{bmatrix}\gamma_N(t) - \boldsymbol{Q}_1\mathbf{z}(t) + \beta\boldsymbol{\gamma}(t). \end{aligned} \tag{20a}$$

$$\dot{\gamma}_N(t) - \beta \cdot \gamma_N(t) = -\partial \boldsymbol{H}_c/\partial z_N(t) = 0 \tag{20b}$$

where

$$\boldsymbol{C}_x = \frac{\partial \mathrm{f}_2(\boldsymbol{z}(t),\boldsymbol{u}(t))}{\partial \mathbf{x}(t)} = \begin{bmatrix} 2\cdot[s_1(t)-s_{min}]\cdot I(s_1(t)-s_{min}) \\ 2\cdot[s_2(t)-s_{min}]\cdot I(s_2(t)-s_{min}) \\ \vdots \\ 2\cdot[s_n(t)-s_{min}]\cdot I(s_n(t)-s_{min}) \end{bmatrix}$$

$$\boldsymbol{C}_y = \frac{\partial \mathrm{f}_2(\boldsymbol{z}(t),\boldsymbol{u}(t))}{\partial \mathbf{y}(t)} = \begin{bmatrix} 2\cdot[v_{max}-v_1(t)]\cdot I(v_{max}-v_1(t)) \\ 2\cdot[v_{max}-v_2(t)]\cdot I(v_{max}-v_2(t)) \\ \vdots \\ 2\cdot[v_{max}-v_n(t)]\cdot I(v_{max}-v_n(t)) \end{bmatrix} + \begin{bmatrix} 2\cdot v_1(t)\cdot I(v_1(t)) \\ 2\cdot v_2(t)\cdot I(v_2(t)) \\ \vdots \\ 2\cdot v_3(t)\cdot I(v_3(t)) \end{bmatrix} + \begin{bmatrix} C_{1,y} \\ C_{2,y} \\ \vdots \\ C_{n,y} \end{bmatrix}$$

$$C_{i,y} = \sum_{j=1}^{i} 2\cdot[s_j(t)-s_{min}]\cdot I(s_j(t)-s_{min}), \forall i = 1,2,\cdots n.$$

The terminal conditions in Eq. (16c) and Eq. (16d) imply that

$$\boldsymbol{\gamma}(T_P) = \boldsymbol{Q}_2\cdot\mathbf{z}(T_P)^T, \gamma_N(T_P) = e^{\beta T_P}\cdot \mathrm{M}\cdot 2\cdot z_N(T_P) \tag{21}$$

Let $\boldsymbol{\gamma}_A^*(t) = \boldsymbol{\lambda}_A^*(t)e^{\beta t}$. Since $e^{\beta t} > 0$, according to Eq. (17), at time t , minimizing $\boldsymbol{H}(\boldsymbol{z}^*(t),\boldsymbol{\lambda}_A^*(t),\boldsymbol{u}(t))$ with respect to $\boldsymbol{u}(t)$ is equivalent to minimizing $\boldsymbol{H_c}(\boldsymbol{z}^*(t),\boldsymbol{\gamma}_A^*(t),\boldsymbol{u}(t))$ with respect to $\boldsymbol{u}(t)$**.** This indicates that if the optimal control $\boldsymbol{u}^*$ minimizes $\boldsymbol{H_c}(\boldsymbol{z}^*(t),\boldsymbol{\lambda}_A^*(t),\boldsymbol{u}(t))$**,** it is the solution to inequality (16e). Thereby, $\boldsymbol{u}^*(t)$ can be found by solving the following minimization problem

$$min_{\boldsymbol{u}(t)}\boldsymbol{H_c}(\boldsymbol{z}^*(t),\boldsymbol{\gamma}_A^*(t),\boldsymbol{u}(t)); \quad \boldsymbol{u}(t),\boldsymbol{u}^*(t) \in \boldsymbol{\mathcal{U}} \tag{22}$$

Proposition 2. *Let* $[p_1(t) \quad p_2(t) \quad \cdots \quad p_n(t)]^T = -(\boldsymbol{R}_3)^{-1}(\boldsymbol{B}^T\boldsymbol{\gamma}^*(t))$*; if* $\boldsymbol{R}_3$ *is a diagonal positive definite matrix, then the optimal control decisions* $\boldsymbol{u}^* = [u_1^* \quad u_2^* \quad \cdots \quad u_n^*]$ *that minimizes* $\boldsymbol{H_c}(\boldsymbol{z}^*,\boldsymbol{\gamma}_A^*,\boldsymbol{u})$ *is unique and can be formulated as*

$$u_i^*(t) = \varphi(\boldsymbol{z}^*(t),\boldsymbol{\gamma}^*(t)) = \begin{cases} u_{min}, if\ p_i(t) < u_{min} \\ u_{max}, if\ p_i(t) > u_{max} \\ p_i(t), if u_{min} \le p_i(t) \le u_{max} \end{cases} \tag{23}$$

Proof. If $\boldsymbol{u}^* = [u_1^* \quad u_2^* \quad \cdots \quad u_n^*]$ minimizes $\boldsymbol{H_c}(\boldsymbol{z}^*(t),\boldsymbol{\gamma}_A^*(t),\boldsymbol{u}(t))$**,** then we have

$$\begin{aligned} &L(\boldsymbol{z}^*(t),\boldsymbol{u}^*(t)) + \boldsymbol{\gamma}^*(t)\mathbf{f}_1(\boldsymbol{z}^*(t),\boldsymbol{u}^*(t)) + \gamma_N^*(t)\mathrm{f}_2(\boldsymbol{z}^*(t),\boldsymbol{u}^*(t)) \\ &\le L(\boldsymbol{z}^*(t),\boldsymbol{u}(t)) + \boldsymbol{\gamma}^*(t)\mathbf{f}_1(\boldsymbol{z}^*(t),\boldsymbol{u}(t)) + \gamma_N^*(t)\mathrm{f}_2(\boldsymbol{z}^*(t),\boldsymbol{u}(t)) \end{aligned} \tag{24}$$

Eq. (24) indicates

$$\begin{aligned} &0.5\cdot\boldsymbol{u}^*(t)^T\boldsymbol{R}_3\boldsymbol{u}^*(t) + (\boldsymbol{\gamma}^*(t))^T\cdot\boldsymbol{B}\cdot\boldsymbol{u}^*(t) \\ &\le 0.5\cdot\boldsymbol{u}(t)^T\boldsymbol{R}_3\boldsymbol{u}(t) + (\boldsymbol{\gamma}^*(t))^T\cdot\boldsymbol{B}\cdot\boldsymbol{u}(t) \end{aligned} \tag{25}$$

Let $\boldsymbol{p}^*(t) = (\boldsymbol{R}_3)^{-1}(\boldsymbol{B}^T\boldsymbol{\gamma}^*(t)) = -[p_1 \quad p_2 \quad \cdots \quad p_n]^T$. Then

$$(\boldsymbol{\gamma}^*(t))^T\cdot\boldsymbol{B}\cdot\boldsymbol{u}^*(t) = (\boldsymbol{u}^*(t))^T\boldsymbol{B}^T\boldsymbol{\gamma}^*(t) = (\boldsymbol{u}^*(t))^T\boldsymbol{R}_3\boldsymbol{p}^*(t) \tag{26a}$$

$$(\boldsymbol{\gamma}^*(t))^T\cdot\boldsymbol{B}\cdot\boldsymbol{u}(t) = (\boldsymbol{u}(t))^T\boldsymbol{B}^T\boldsymbol{\gamma}^*(t) = (\boldsymbol{u}(t))^T\boldsymbol{R}_3\boldsymbol{p}^*(t) \tag{26b}$$

Substituting Eq. (26) into Eq. (25), we have

$$\begin{aligned} &0.5\cdot\boldsymbol{u}^*(t)^T\boldsymbol{R}_3\boldsymbol{u}^*(t) + (\boldsymbol{u}^*(t))^T\boldsymbol{R}_3\boldsymbol{p}^*(t) \\ &\le 0.5\cdot\boldsymbol{u}(t)^T\boldsymbol{R}_3\boldsymbol{u}(t) + (\boldsymbol{u}(t))^T\boldsymbol{R}_3\boldsymbol{p}^*(t) \end{aligned} \tag{27}$$

Adding $0.5\cdot\boldsymbol{p}^*(t)^T\boldsymbol{R}_3\boldsymbol{p}^*(t) = 0.5(\boldsymbol{\gamma}^*(t))^T\cdot\boldsymbol{B}(\boldsymbol{R}_3)^{-1}\boldsymbol{B}^T\boldsymbol{\gamma}^*(t)$ to both sides of inequality (27), we have

$$0.5[\boldsymbol{u}^*(t)+\boldsymbol{p}^*(t)]^T\boldsymbol{R}_3[\boldsymbol{u}^*(t)+\boldsymbol{p}^*(t)] \le 0.5[\boldsymbol{u}(t)+\boldsymbol{p}^*(t)]^T\boldsymbol{R}_3[\boldsymbol{u}(t)+\boldsymbol{p}^*(t)] \quad (28)$$

Inequality (28) implies that if $\boldsymbol{u}^*$ minimizes $\boldsymbol{H_c}(\boldsymbol{z}^*(t), \boldsymbol{\gamma}_A^*(t), \boldsymbol{u}(t))$, it must minimize inequality (27) and vice versa. Thereby

$$\boldsymbol{u}^*(t) = min_{\boldsymbol{u}\in\boldsymbol{U}}[\boldsymbol{u}(t)+\boldsymbol{p}^*(t)]^T\boldsymbol{R}_3[\boldsymbol{u}(t)+\boldsymbol{p}^*(t)] \quad (29)$$

Note $\boldsymbol{R}_3$ is a diagonal positive definite matrix; without loss of generosity, let $\boldsymbol{R}_3 = diag([w_1, w_2 \cdots, w_n])$, $w_i > 0, \forall i = 1,2,\cdots,n$. Then, inequality (29) can be written as

$$\begin{aligned}\boldsymbol{u}^*(t) &= min_{\boldsymbol{u}\in\boldsymbol{U}} \sum_{i=1}^{n} w_i[u_i(t)-p_i]^2 \\ &= \sum_{i=1}^{n} min_{u_{min}\le u_i \le u_{max}} w_i[u_i(t)-p_i]^2\end{aligned} \quad (30)$$

The only solution to the above inequality is

$$u_i^*(t) = \begin{cases} u_{min}, if\ p_i(t) < u_{min} \\ u_{max}, if\ p_i(t) > u_{max} \\ p_i(t), if u_{min} \le p_i(t) \le u_{max} \end{cases} ; \forall i = 1,2,\cdots,n \quad (31)$$

This completes the proof. ■

Eq. (13b), Eq. (13c), Eq. (20a), Eq. (20b) and Eq. (23) form a two-point boundary value problem as follows with initial conditions and terminal conditions provided by Eq.(12e) and Eq. (21), respectively.

$$\dot{\mathbf{z}}(t) = \boldsymbol{A}\cdot\mathbf{z}(t) + \boldsymbol{B}\cdot\varphi\big(\boldsymbol{z}(t), \boldsymbol{\gamma}(t)\big) \quad (32a)$$

$$\dot{z}_N(t) = \sum_{i=1}^{n}\left(z_{N,1}^i + z_{N,2}^i + z_{N,3}^i\right) \quad (32c)$$

$$\dot{\boldsymbol{\gamma}}(t) = -\boldsymbol{A}\cdot\boldsymbol{\gamma}(t) - \begin{bmatrix}\boldsymbol{C}_x \\ \boldsymbol{C}_y\end{bmatrix}\gamma_N(t) - \boldsymbol{Q}_1\mathbf{z}(t) + \beta\boldsymbol{\gamma}(t) \quad (32d)$$

$$\dot{\gamma}_N(t) = \beta\cdot\gamma_N(t) \quad (32e)$$

$$\mathbf{z}(0) = [\mathbf{x}_0^T \quad \mathbf{y}_0^T]^T; z_N(0) = 0; \quad (32f)$$

$$\boldsymbol{\gamma}(T_P) = \boldsymbol{Q}_2\mathbf{z}(T_P), \gamma_N(T_P) = e^{\beta T_P}\cdot \mathrm{M}\cdot 2\cdot z_N(T_P) \quad (32g)$$

The two-point boundary value problem can be solved using many existing solution algorithms. A review of these algorithms is provided in Kirk (2012). In this study, the shooting method is used to solve the two-point boundary value problem (32). The details of implementing the shooting method can be found in Keller (1976). The main advantage of the shooting method is that it converges very fast if the algorithm starts to converge (Keller, 1976). Note, $\partial^2\boldsymbol{H_c}/\partial(\boldsymbol{u}(t))^2 = \boldsymbol{R}_3$ is a positive definite matrix. Thereby, the solution $(\boldsymbol{z}^*(t), z_N^*(t), \boldsymbol{\gamma}^*(t), \gamma_N^*(t))$ of the two-point boundary value problem (32) is a minimum solution of optimal control problem (5). The optimal control $\boldsymbol{u}^*(t)$ can be obtained by inputting $\boldsymbol{\gamma}^*(t)$ into Eq. (23).

4. Sensitivity analysis of the optimal control problem

For the DMPC approach, at each sampling time instant t_k, the control decisions are determined by solving the two-point boundary value problem (32) with the predicted spacing error and relative speed of vehicle 1 with respect to the leading vehicle (i.e., $\hat{x}_1(t_k)$ and $\hat{y}_1(t_k)$). The resulting control decisions

may deviate significantly from those of the idealized MPC strategy due to errors in predicting f $x_1(t_k)$ and $y_1(t_k)$, which can decrease the platoon performance and cause collisions. To address this issue, the DMPC-FOA approach corrects the estimated control decisions of the DMPC approach using first-order Taylor approximation. To do so, the main step is to obtain the derivatives of the optimal solution of the state and costate variables with respect to $\tilde{x}_1(t_k)$ and $\tilde{y}_1(t_k)$ in the DMPC-FOA approach, respectively.

The sensitivity analysis of an optimal control problem quantitatively measures the change in the optimal solution of the state and costate variables induced by a unit change in the perturbed parameters (i.e., $\tilde{x}_1(t_k)$ and $\tilde{y}_1(t_k)$ in this study). Parametric sensitivity of optimal problem has been extensively studied. Dorato (1963) developed an analytical model to study the variation of the objective function with respect to parametric perturbations. Malanowski (1984, 1987) discussed the conditions for directional differentiability of the solutions for an optimal control problem with nonlinear ordinary dynamics. Maurer and Pesch (1984) developed an analytical method for sensitivity analysis of optimal control problems with no constraints. This method is further extended to study the sensitivity analysis of optimal control problems with control constraints (Maurer and Pesch, 1995; Malanowski and Maurer, 1996), and pure state variable constraints (Augustin and Maurer, 2001; Malanowski, 2011). Here, the analytical method for sensitivity analysis of the optimal control decisions with respect to $\tilde{x}_1(t_k)$ and $\tilde{y}_1(t_k)$ will be derived by modifying the method developed by Maurer and Pesch (1995) for a general optimal control problem.

Denote $\widetilde{\boldsymbol{u}}^*(t) = [\tilde{u}_1^*(t), \cdots, \tilde{u}_n^*(t)]$ as the control decisions obtained by solving Eq. (32) using $\tilde{x}_1(t_k)$ and $\tilde{y}_1(t_k)$ predicted by the DMPC-FOA approach. The corresponding solutions for the state variables (i.e., $\mathbf{z}(t)$, $z_N(t)$) and costate variables (i.e., $\boldsymbol{\gamma}(t)$, $\gamma(t)$) are denoted as $\tilde{\mathbf{z}}^*(t)$, $\tilde{z}_N^*(t)$, $\tilde{\boldsymbol{\gamma}}^*(t)$ and $\tilde{\gamma}_N^*(t)$, respectively. Let the derivatives of the optimal solutions for the state and costate variables with respect to $\tilde{x}_1(t_k)$ be defined as follows:

$$\mathbf{h}_{\tilde{x}_1}(t) = \frac{\partial \tilde{\mathbf{z}}^*(t)}{\partial \tilde{x}_1(t_k)};\ h_{N,\tilde{x}_1}(t) = \frac{\partial \tilde{z}_N^*(t)}{\partial \tilde{x}_1(t_k)}$$

$$\boldsymbol{\eta}_{\tilde{x}_1}(t) = \frac{\partial \tilde{\boldsymbol{\gamma}}^*(t)}{\partial \tilde{x}_1(t_k)};\ \eta_{N,\tilde{x}_1}(t) = \frac{\partial \tilde{\gamma}_N^*(t)}{\partial \tilde{x}_1(t_k)}.$$

According to $\tilde{u}_i^*(t)$, we can obtain the set of time intervals $\Omega_{i,1}$, $\Omega_{i,2}$, and $\Omega_{i,2}$ ($\Omega_{i,1} \cup \Omega_{i,2} \cup \Omega_{i,2} = [0, T_P]$) for each vehicle $i, i = 1,2,\cdots,n$ such that

$$\tilde{u}_i^*(t) = \begin{cases} u_{min}, t \in \Omega_{i,1} \\ u_{max}, t \in \Omega_{i,2} \\ \tilde{p}_i, t \in \Omega_{i,3} \end{cases} \tag{33}$$

where $[\tilde{p}_1(t) \quad \tilde{p}_2(t) \quad \cdots \quad \tilde{p}_n(t)]^T = -(\boldsymbol{R}_3)^{-1}(\boldsymbol{B}^T\tilde{\boldsymbol{\gamma}}^*(t))$.

Then, according to Eq. (33), we have

$$\frac{d\tilde{u}_i^*(t)}{d\tilde{x}_1(t_k)} = \begin{cases} 0, t \in \left(\Omega_{i,1} \cup \Omega_{i,2}\right) \\ m_{\tilde{x}_1,i}(t), t \in \Omega_{i,3} \end{cases} \tag{34a}$$

where

$$[m_{\tilde{x}_1,1}(t) \quad m_{\tilde{x}_1,2}(t) \quad \cdots \quad m_{\tilde{x}_1,n}(t)]^T = -(\boldsymbol{R}_3)^{-1}\left(\boldsymbol{B}^T\,\boldsymbol{\eta}_{\tilde{x}_1}(t)\right). \tag{34b}$$

Let $\Psi\left(\boldsymbol{\eta}_{\tilde{x}_1}(t)\right) = \left[\frac{d\tilde{u}_1^*(t)}{d\tilde{x}_1(t_k)} \quad \frac{d\tilde{u}_2^*(t)}{d\tilde{x}_1(t_k)} \quad \cdots \quad \frac{d\tilde{u}_n^*(t)}{d\tilde{x}_1(t_k)}\right]^T$. Differentiating both sides of Eqs. (32a)-(32g) with respect to $\tilde{x}_1(t_k)$, we have

$$\dot{\mathbf{h}}_{\tilde{x}_1}(t) = \boldsymbol{A} \cdot \mathbf{h}_{\tilde{x}_1} + \boldsymbol{B} \cdot \Psi\big(\boldsymbol{\eta}_{\tilde{x}_1}(t)\big) \tag{35a}$$

$$\dot{h}_{N,\tilde{x}_1} = \begin{bmatrix} \boldsymbol{C}_x^T & \boldsymbol{C}_y^T \end{bmatrix} \cdot \mathbf{h}_{\tilde{x}_1} \tag{35c}$$

$$\dot{\boldsymbol{\eta}}_{\tilde{x}_1} = -\boldsymbol{A} \cdot \boldsymbol{\eta}_{\tilde{x}_1}(t) - \begin{bmatrix} \boldsymbol{C}_x \\ \boldsymbol{C}_y \end{bmatrix} \eta_{N,\tilde{x}_1}(t) - \boldsymbol{Q}_1 \mathbf{h}_{\tilde{x}_1} + \beta \boldsymbol{\eta}_{\tilde{x}_1}(t) \tag{35d}$$

$$\dot{\eta}_{N,\tilde{x}_1}(t) = \beta \cdot \eta_{N,\tilde{x}_1}(t) \tag{35e}$$

with initial and terminal conditions as:

$$\mathbf{h}_{\tilde{x}_1}(0) = \frac{\partial \tilde{\mathbf{z}}(0)}{\partial \tilde{x}_1(t_k)} = \frac{\partial \tilde{\mathbf{z}}(t_k)}{\partial \tilde{x}_1(t_k)} = [1, \mathbf{0}_{1\times 2n-1}]^T \tag{35f}$$

$$h_{N,\tilde{x}_1}(0) = \frac{\partial \tilde{z}_N(0)}{\partial \tilde{x}_1(t_k)} = \frac{\partial(0)}{\partial \tilde{x}_1(t_k)} = 0 \tag{35g}$$

$$\boldsymbol{\eta}_{\tilde{x}_1}(T_P) = \frac{\partial \tilde{\boldsymbol{\gamma}}_1(T_P)}{\partial \tilde{x}_1(t_k)} = \frac{\partial(\boldsymbol{Q}_2 \tilde{\mathbf{z}}(T_P))}{\partial \tilde{x}_1(t_k)} = \boldsymbol{Q}_2 \cdot \mathbf{h}_{\tilde{x}_1}(T_P) \tag{35h}$$

$$\eta_{N,\tilde{x}_1}(T_P) = \frac{\partial \tilde{\gamma}_N(T_P)}{\partial \tilde{x}_1(t_k)} = \frac{\partial\big(e^{\beta T_P} \cdot \mathrm{M} \cdot 2 \cdot \tilde{z}_N(T_P)\big)}{\partial \tilde{x}_1(t_k)} = e^{\beta T_P} \cdot \mathrm{M} \cdot 2 \cdot h_{N,\tilde{x}_1}(T_P) \tag{35i}$$

where $\mathbf{0}_{1\times 2n-1}$ is a $(2n-1)$-dimensional zero vector. Eqs. (35a)-(35i) also form a two-point boundary value problem which can be solved using the shooting method.

To obtain the derivatives of the optimal state and costate variables with respect to $\tilde{y}_1(t_k)$, similarly, let

$$\mathbf{h}_{\tilde{y}_1}(t) = \frac{\partial \tilde{\mathbf{z}}^*(t)}{d\tilde{y}_1(t_k)};\ \ h_{N,\tilde{y}_1}(t) = \frac{\partial \tilde{z}_N^*(t)}{d\tilde{y}_1(t_k)} \tag{36a}$$

$$\boldsymbol{\eta}_{\tilde{y}_1}(t) = \frac{\partial \tilde{\boldsymbol{\gamma}}^*(t)}{\partial \tilde{y}_1(t_k)};\ \eta_{N,\tilde{y}_1}(t) = \frac{\partial \tilde{\gamma}_N^*(t)}{\partial \tilde{y}_1(t_k)}. \tag{36b}$$

Differentiating both sides of Eqs. (32a)-(32f) with respect to $\tilde{y}_1(t_k)$, we can obtain a similar two-point boundary value problem, as follows:

$$\dot{\mathbf{h}}_{\tilde{y}_1}(t) = \boldsymbol{A} \cdot \mathbf{h}_{\tilde{y}_1} + \boldsymbol{B} \cdot \Psi\big(\boldsymbol{\eta}_{\tilde{y}_1}(t)\big) \tag{37a}$$

$$\dot{h}_{N,\tilde{y}_1} = \begin{bmatrix} \boldsymbol{C}_x^T & \boldsymbol{C}_y^T \end{bmatrix} \mathbf{h}_{\tilde{y}_1} \tag{37c}$$

$$\dot{\boldsymbol{\eta}}_{\tilde{y}_1} = -\boldsymbol{A} \cdot \boldsymbol{\eta}_{\tilde{y}_1}(t) - \begin{bmatrix} \boldsymbol{C}_x \\ \boldsymbol{C}_y \end{bmatrix} \eta_{N,\tilde{y}_1}(t) - \boldsymbol{Q}_1 \mathbf{h}_{\tilde{y}_1} + \beta \boldsymbol{\eta}_{\tilde{y}_1}(t) \tag{37d}$$

$$\dot{\eta}_{N,\tilde{y}_1}(t) = \beta \cdot \eta_{N,\tilde{y}_1}(t) \tag{37e}$$

with initial and terminal conditions as:

$$\mathbf{h}_{\tilde{y}_1}(0) = \frac{\partial \tilde{\mathbf{z}}(0)}{\partial \tilde{y}_1(t_k)} = \frac{\partial \tilde{\mathbf{z}}(t_k)}{\partial \tilde{y}_1(t_k)} = [\mathbf{0}_{1\times n}, 1, \mathbf{0}_{1\times n-1}]^T \tag{37f}$$

$$h_{N,\tilde{y}_1}(0) = \frac{\partial \tilde{z}_N(0)}{\partial \tilde{y}_1(t_k)} = \frac{\partial(0)}{\partial \tilde{y}_1(t_k)} = 0 \tag{37g}$$

$$\boldsymbol{\eta}_{\tilde{y}_1}(T_P) = \frac{\partial \tilde{\boldsymbol{\gamma}}_1(T_P)}{\partial \tilde{y}_1(t_k)} = \frac{d(\boldsymbol{Q}_2 \tilde{\mathbf{z}}(T_P))}{\partial \tilde{y}_1(t_k)} = \boldsymbol{Q}_2 \cdot \mathbf{h}_{\tilde{y}_1}(T_P) \tag{37h}$$

$$\eta_{N,\tilde{y}_1}(T_P)=\frac{\partial\tilde{\gamma}_N(T_P)}{\partial\tilde{y}_1(t_k)}=\frac{\partial\left(e^{\beta T_P}\cdot \mathrm{M}\cdot 2\cdot\tilde{z}_N(T_P)\right)}{\partial\tilde{y}_1(t_k)}=e^{\beta T_P}\cdot \mathrm{M}\cdot 2\cdot h_{N,\tilde{y}_1}(T_P) \tag{37i}$$

where $\mathbf{0}_{1\times n-1}$ is a $(n-1)$-dimensional zero vector. The vector of functions $\Psi\left(\boldsymbol{\eta}_{\tilde{y}_1}(t)\right)$ is similar to $\Psi\left(\boldsymbol{\eta}_{\tilde{x}_1}(t)\right)$. It is formulated by replacing the subscript "$\tilde{x}_1$" in Eq. (34) with "$\tilde{y}_1$".

The derivatives of the optimal solutions for the state and costate variables with respect to $\tilde{x}_1(t_k)$ and $\tilde{y}_1(t_k)$ can be obtained by solving the two-point boundary value problems (35) and (37), respectively. Then, when the actual value of $x_1(t_k)$ and $y_1(t_k)$ are detected at the sampling time instant t_k, the optimal solution of the state and costate variables of the idealized MPC strategy can be estimated using first-order Taylor approximation, as follows

$$\bar{\boldsymbol{z}}^*(t)=\tilde{\boldsymbol{z}}^*(t)+\mathbf{h}_{\tilde{x}_1}(t)\left(x_1(t_k)-\tilde{x}_1(t_k)\right)+\mathbf{h}_{\tilde{y}_1}(t)\left(y_1(t_k)-\tilde{y}_1(t_k)\right) \tag{38a}$$

$$\bar{\boldsymbol{\gamma}}^*(t)=\tilde{\boldsymbol{\gamma}}^*(t)+\boldsymbol{\eta}_{\tilde{x}_1}(t)\left(x_1(t_k)-\tilde{x}_1(t_k)\right)+\boldsymbol{\eta}_{\tilde{y}_1}(t)\left(y_1(t_k)-\tilde{y}_1(t_k)\right) \tag{38b}$$

Eq. (38a) and Eq. (38b) can be calculated instantaneously at the sampling time instant t_k as $\mathbf{h}_{\tilde{x}_1}(t)$, $\mathbf{h}_{\tilde{y}_1}(t)$, $\boldsymbol{\eta}_{\tilde{x}_1}(t)$ and $\boldsymbol{\eta}_{\tilde{y}_1}(t)$ are obtained before t_k. Eq. (38) indicates that compared to $[\tilde{\boldsymbol{z}}^*(t),\tilde{\boldsymbol{\gamma}}^*(t)]$, $[\bar{\boldsymbol{z}}^*(t),\bar{\boldsymbol{\gamma}}^*(t)]$ are closer to $[\boldsymbol{z}^*(t),\boldsymbol{\gamma}^*(t)]$ calculated for the idealized MPC strategy using exact $x_1(t_k)$ and $y_1(t_k)$. According to Eq. (23), the optimal control decisions of the idealized MPC strategy can be estimated as

$$\bar{u}_i^*(t)=\varphi\left(\bar{\boldsymbol{z}}^*(t),\bar{\boldsymbol{\gamma}}^*(t)\right)=\begin{cases}u_{min}, if\ \bar{p}_i(t)<u_{min}\\ u_{max}, if\ \bar{p}_i(t)>u_{max}\\ \bar{p}_i(t), if u_{min}\le\ \bar{p}_i(t)\le u_{max}\end{cases};\forall i=1,2,\cdots,n \tag{39}$$

where $[\bar{p}_1(t)\quad \bar{p}_2(t)\quad \cdots\quad \bar{p}_n(t)]^T=-(\boldsymbol{R}_3)^{-1}(\boldsymbol{B}^T\bar{\boldsymbol{\gamma}}^*(t))$. Compared to $\tilde{\boldsymbol{u}}^*(t)$, the estimated $\bar{\boldsymbol{u}}^*(t),(\bar{\boldsymbol{u}}^*(t)=[\bar{u}_1^*(t)\quad \bar{u}_2^*(t)\quad \cdots\quad \bar{u}_n^*(t)]^T)$ is closer to $\boldsymbol{u}^*(t)$ calculated using the idealized MPC strategy as $\bar{\boldsymbol{\gamma}}^*(t)$ is closer to $\boldsymbol{\gamma}^*(t)$ compared to $\tilde{\boldsymbol{\gamma}}^*(t)$.

Proposition 3: *If the inequality constraints (5c), (5d) and (5e) are not active along the trajectory of the optimal solution* $(\tilde{\boldsymbol{z}}^*(t),\tilde{z}^*(t),\tilde{\boldsymbol{\gamma}}^*(t),\tilde{\gamma}^*(t))$ *obtained with the predicted initial state* $\tilde{x}_1(t_k)$ *and* $\tilde{y}_1(t_k)$, *then the derivatives of optimal solutions for the state and costate variables with respect to* $\tilde{x}_1(t_k)$ *and* $\tilde{y}_1(t_k)$ *are the same for all solutions of* $(\tilde{\boldsymbol{z}}^*(t),\tilde{z}^*(t),\tilde{\boldsymbol{\gamma}}^*(t),\tilde{\gamma}^*(t))$ *for which the inequality constraints (5c) and (5d) are not active.*

Proof: If the inequality constraints (5c), (5d) and (5e) are not active along the optimal solution, $\tilde{z}_N^*(t)\equiv 0$, $t\in[0,T_P]$. According to Eq. (16d), $\tilde{\gamma}_N^*(T_P)=2\,\mathrm{M}\cdot\tilde{z}_N^*(T_P)=2\,\mathrm{M}\cdot 0=0$. Based on Eq. (32e), $\tilde{\gamma}_N^*(t)\equiv 0, t\in[0,T_P]$. This indicates that $\eta_{N,\tilde{x}_1}(t)=\eta_{N,\tilde{y}_1}(t)\equiv 0, t\in[0,T_P]$. In addition, $\Psi\left(\boldsymbol{\eta}_{\tilde{x}_1}(t)\right)=-(\boldsymbol{R}_3)^{-1}\left(\boldsymbol{B}^T\boldsymbol{\eta}_{\tilde{x}_1}(t)\right)$ and $\Psi\left(\boldsymbol{\eta}_{\tilde{y}_1}(t)\right)=-(\boldsymbol{R}_3)^{-1}\left(\boldsymbol{B}^T\boldsymbol{\eta}_{\tilde{y}_1}(t)\right)$. Thereby, the two-point boundary value problems (35) and (37) are the same for different optimal solutions under which the inequality constraints (5c), (5d) and (5e) are not active. This indicates that the derivatives of the optimal solutions for the state and costate variables with respect to $\tilde{x}_1(t_k)$ and $\tilde{y}_1(t_k)$ are the same for all of these solutions. ■

Proposition 3 implies that if under the optimal control decisions, the following vehicles in the platoon do not brake and accelerate at the maximum values, the speed is within the speed limit, and the spacing between all adjacent vehicle pairs is larger than the minimum spacing during time interval $[t_k,t_k+T_P]$,

the changes in the optimal control decisions for a unit change in $\tilde{x}_1(t_k)$ and $\tilde{y}_1(t_k)$ would be the same for all of these optimal control decisions. It is worth noting that the idealized MPC strategy can coordinate the behaviors of all following vehicles to minimize the objective function efficiently. It can enable smoother deceleration and acceleration behavior of all following vehicles even if the leading vehicle decelerates or accelerates at the maximum value. The following vehicles accelerate or decelerate at the maximum value only when the spacing between two consecutive vehicles is too large or too small. Thereby, according to Proposition 3, under normal conditions, the derivatives of the optimal solutions for the state and costate variables, i.e., $(\tilde{\boldsymbol{z}}(t), \tilde{z}_N(t), \tilde{\boldsymbol{\gamma}}(t), \tilde{\gamma}_N(t))$ with respect to $\tilde{x}_1(t_k)$ and $\tilde{y}_1(t_k)$ are the same and are independent of these solutions. Let $\mathbf{h}_l^*(t), h_{N,l}^*(t), \boldsymbol{\eta}_l^*(t), \eta_{N,l}^*(t), l \in \{\tilde{x}_1, \tilde{y}_1\}, t \in [0, T_P]$ be the corresponding derivatives. These derivatives can be obtained offline to avoid solving the two-point boundary value problems (35) and (37) in real time. Thereby, under normal situations when the inequality constraints (5c), (5d) and (5e) are not active along the optimal solution, the time reserved for computing in DMPC-FOA approach can be the same as that of the DMPC approach.

Further, when the inequality constraints are active frequently for some traffic flow conditions (e.g., very congested flow), the two-point boundary value problems (35) and (37) need to be solved in real time. $\mathbf{h}_l^*(t), h_{N,l}^*(t), \boldsymbol{\eta}_l^*(t), \eta_{N,l}^*(t), l \in \{\tilde{x}_1, \tilde{y}_1\}, t \in [0, T_P]$ can be used as the initial point for the shooting method to solve the two-point boundary value problems. This can significantly reduce the computational time for solving the two problems as they are closer to the optimal solution. This property enhances the applicability of the proposed DMPC-FOA approach for controlling the CAV platoon in real-time.

5. Stability analysis of the idealized MPC strategy with no inequality constraints

Stability is an important property for a CAV platoon. It indicates the capability of a platoon to recover to a stable state after external disturbances on the platoon formation (e.g., unexpected hard acceleration and deceleration of the leading vehicle). In this study, the condition for asymptotic stability of the idealized MPC strategy is analyzed to ensure that the CAV platoon can dampen traffic oscillations efficiently. This condition also ensures the local stability of the DMPC-FOA approaches as it is proposed to characterize the control decisions of the idealized MPC strategy. Similar to Gong et al., (2016), the stability analysis of the idealized MPC strategy is based on optimal control problem (5) with no inequality constraints as they are not active in most traffic flow scenarios. The conditions for asymptotic stability of the idealized MPC strategy with active constraints will be investigated in our future work.

For convenience of stability analysis, in the following, optimal control problem (5) without inequality constraints (5c) and (5d) is transformed into an equivalent form for analyzing stability. The conditions for asymptotic stability of the unconstrained idealized MPC strategy are analyzed using the stability theorem for continuous MPC problems developed by Mayne et.al. (2000). Let

$$\boldsymbol{z}_\beta(t) = e^{-\frac{\beta}{2}t}\boldsymbol{z}(t) \tag{40a}$$

$$\boldsymbol{u}_\beta(t) = e^{-\frac{\beta}{2}t}\boldsymbol{u}(t) \tag{40b}$$

Then, optimal control problem (5) without inequality constraints (5c) and (5d) can be formulated as

$$\min_{\boldsymbol{u}_\beta} \int_0^{T_P} \left[\boldsymbol{z}_\beta(t)^T \boldsymbol{Q}_1 \boldsymbol{z}_\beta(t) + \boldsymbol{u}_\beta(t)^T \boldsymbol{R}_3 \boldsymbol{u}_\beta(t)\right] dt + \boldsymbol{z}_\beta(T_P)^T \boldsymbol{Q}_2 \boldsymbol{z}_\beta(T_P) \tag{41a}$$

$$s.t\ \dot{\boldsymbol{z}}_\beta(t) = \left(\boldsymbol{A} - \frac{\beta}{2}\boldsymbol{E}_{2n}\right)\boldsymbol{z}_\beta(t) + \boldsymbol{B}\boldsymbol{u}_\beta(t) \quad (41b)$$

$$\boldsymbol{z}_\beta(0) = [\mathbf{x}_k \quad \mathbf{y}_k]^T \quad (41c)$$

The following theorem is used to analyze the asymptotical stability of the idealized MPC strategy with no inequality constraints.

Theorem 1 (Mayne et.al. 2000): *Consider the following continuous constrained MPC problem*

$$\min_{\boldsymbol{a}} \int_0^{T_P} L(\boldsymbol{z}(t), \boldsymbol{u}(t))\, dt + F(\boldsymbol{z}(T_P))$$

$$s.t \quad \dot{\boldsymbol{z}} = g(\boldsymbol{z}, \boldsymbol{u})$$
$$\boldsymbol{z}(t) \in \mathcal{Z}, \quad for\ t\epsilon[0, T_P]$$
$$\boldsymbol{u}(t) \in \mathcal{A}, \quad for\ t\epsilon[0, T_P]$$
$$\boldsymbol{z}(T_P) \in \mathcal{Z}_f$$

where $\boldsymbol{z}$ and $\boldsymbol{u}$ are vectors of the state variables and control variables, respectively. $\boldsymbol{z}(T_P)$ is the value of $\boldsymbol{z}(t)$ at terminal time T_P. $\mathcal{Z}$, $\mathcal{A}$, and $\mathcal{Z}_f$ are the feasible sets for $\boldsymbol{z}(t)$, $\boldsymbol{u}(t)$ and $\boldsymbol{z}(T_P)$, respectively. If there exists a nominal controller $\kappa(\boldsymbol{z})$ such that the following four conditions hold for the above continuous MPC problem, then it is asymptotic stable.

(1). $0 \in \mathcal{Z}$

(2). $\kappa(\boldsymbol{z}) \in \mathcal{A}, \forall \boldsymbol{z} \in \mathcal{Z}_f$

(3). $g(\boldsymbol{z}, \kappa(\boldsymbol{z})) \in \mathcal{Z}_f$ *for* $\forall \boldsymbol{z} \in \mathcal{Z}_f$

(4). $\left[\dot{F} + L\right](\boldsymbol{z}, \kappa(\boldsymbol{z})) \leq 0$ *for* $\forall \boldsymbol{z} \in \mathcal{Z}_f$

To enable application of Theorem 1 for stability analysis of the unconstrained idealized MPC strategy based on optimal control problem (41), let

$$\boldsymbol{z}(t) = \boldsymbol{z}_\beta(t) \quad (42a)$$

$$\boldsymbol{u}(t) = \boldsymbol{u}_\beta(t) \quad (42b)$$

$$\dot{\boldsymbol{z}}(t) = g(\boldsymbol{z}, \boldsymbol{u}) = \left(\boldsymbol{A} - \frac{\beta}{2}\boldsymbol{E}_{2n}\right)\boldsymbol{z}(\boldsymbol{t}) + \boldsymbol{B}\boldsymbol{u}(t) \quad (42c)$$

$$L\big(\boldsymbol{z}(t), \boldsymbol{u}(t)\big) = \boldsymbol{z}(\boldsymbol{t})^T\boldsymbol{Q}_1\boldsymbol{z}(\boldsymbol{t}) + \boldsymbol{u}(t)^T\boldsymbol{R}_3\boldsymbol{u}(t) \quad (42d)$$

$$F\big(\boldsymbol{z}(t)\big) = \boldsymbol{z}(t)^T\boldsymbol{Q}_2\boldsymbol{z}(t) \quad (42e)$$

$$\dot{F}\big(\boldsymbol{z}(t)\big) = \dot{\boldsymbol{z}}(t)^T\boldsymbol{Q}_2\boldsymbol{z}(t) + \boldsymbol{z}(t)^T\boldsymbol{Q}_2\dot{\boldsymbol{z}}(t) \quad (42f)$$

This study chooses a linear nominal controller (Camacho and Alba, 2013) as follows

$$\kappa(\boldsymbol{z}) = \boldsymbol{\mathcal{K}}\boldsymbol{z} \quad (43)$$

Let $\boldsymbol{\mathcal{K}} = \mathbf{0}_{2n\times n}$**.** This choice of matrix $\boldsymbol{\mathcal{K}}$ will simplify the analysis of conditions for asymptotic stability of the unconstrained idealized MPC strategy based on optimal control problem (41). Next, we illustrate the conditions for which optimal control problem (41) can satisfy the four conditions in Theorem 1.

For optimal control problem (41), the feasible set of state variables, control variables, and terminal state variables are $\mathcal{Z} = \mathbb{R}^{2n}$, $\mathcal{A} = \mathbb{R}^n$, and $\mathcal{Z}_f = \mathbb{R}^{2n}$, respectively. Thereby, $0 \in \mathcal{Z}$; condition 1 is satisfied. According to Eq. (43), $\kappa(\boldsymbol{z}) = \boldsymbol{\mathcal{K}}\boldsymbol{z} = \mathbf{0}_{1\times n} \in \mathbb{R}^n = \mathcal{A}$. Hence, condition 2 in Theorem 1 is also satisfied. From Eq. (42c) and Eq. (43), $g\big(\boldsymbol{z}, \kappa(\boldsymbol{z})\big) = \left(\boldsymbol{A} - \frac{\beta}{2}\boldsymbol{E}_{2n}\right)\boldsymbol{z}(t) + \boldsymbol{B}\boldsymbol{\mathcal{K}}\boldsymbol{z}(t) = \left(\boldsymbol{A} - \frac{\beta}{2}\boldsymbol{E}_{2n}\right)\boldsymbol{z}(t) \in \mathbb{R}^{2n} = \mathcal{Z}_f$. Therefore, condition 3 holds for optimal control problem (41).

To illustrate that condition 4 is satisfied, for simplicity, the notation for time t is removed. Substituting Eqs. (42c)-(42f) into the inequality in condition 4, we have

$$\left[\left(\boldsymbol{A}-\frac{\beta}{2}\boldsymbol{E}_{2n}\right)\boldsymbol{z}+\boldsymbol{B}\boldsymbol{\mathcal{K}}\boldsymbol{z}\right]^{T}\boldsymbol{Q}_2\boldsymbol{z}+\boldsymbol{z}^{T}\boldsymbol{Q}_2\left[\left(\boldsymbol{A}-\frac{\beta}{2}\boldsymbol{E}_{2n}\right)\boldsymbol{z}+\boldsymbol{B}\boldsymbol{\mathcal{K}}\boldsymbol{z}\right]+\boldsymbol{z}^{T}\boldsymbol{Q}_1\boldsymbol{z} + (\boldsymbol{\mathcal{K}}\boldsymbol{z})^{T}\boldsymbol{R}_3(\boldsymbol{\mathcal{K}}\boldsymbol{z})\le 0 \tag{44}$$

Note $\boldsymbol{\mathcal{K}}=\boldsymbol{0}_{2n\times n}$; hence, inequality (44) can be simplified as

$$\boldsymbol{z}^{T}\left[\left(\boldsymbol{A}-\frac{\beta}{2}\boldsymbol{E}_{2n}\right)^{T}\boldsymbol{Q}_2+\boldsymbol{Q}_2\left(\boldsymbol{A}-\frac{\beta}{2}\boldsymbol{E}_{2n}\right)+\boldsymbol{Q}_1\right]\boldsymbol{z}\le 0 \tag{45}$$

Let $\boldsymbol{W}=\left(\boldsymbol{A}-\frac{\beta}{2}\boldsymbol{E}_{2n}\right)^{T}\boldsymbol{Q}_2+\boldsymbol{Q}_2\left(\boldsymbol{A}-\frac{\beta}{2}\boldsymbol{E}_{2n}\right)+\boldsymbol{Q}_1$. Obviously, inequality (45) holds if matrix $\boldsymbol{W}$ is negative semidefinite. According to Eq. (6), $\boldsymbol{R}_1=\boldsymbol{\Lambda}^{\boldsymbol{T}}\boldsymbol{D}_a\boldsymbol{\Lambda}$, $\boldsymbol{R}_2=\boldsymbol{\Lambda}^{\boldsymbol{T}}\boldsymbol{D}_b\boldsymbol{\Lambda}$, $\boldsymbol{R}_4=\boldsymbol{\Lambda}^{\boldsymbol{T}}\boldsymbol{D}_c\boldsymbol{\Lambda}$, and $\boldsymbol{R}_5=\boldsymbol{\Lambda}^{\boldsymbol{T}}\boldsymbol{D}_e\boldsymbol{\Lambda}$, where $\boldsymbol{\Lambda}$ is an $n\times n$ orthogonal matrix and $\boldsymbol{\Lambda}^{T}\boldsymbol{\Lambda}=\boldsymbol{\Lambda}\boldsymbol{\Lambda}^{T}=\boldsymbol{E}_n$. Let the diagonal positive definite matrices $\boldsymbol{D}_a$, $\boldsymbol{D}_b$, $\boldsymbol{D}_c$ and $\boldsymbol{D}_e$ be $\boldsymbol{D}_a=\mathrm{diag}(a_1,\dots,a_n)$, $\boldsymbol{D}_b=\mathrm{diag}(b_1,\dots,b_n)$, $\boldsymbol{D}_c=\mathrm{diag}(c_1,\dots,c_n)$, and $\boldsymbol{D}_e=\mathrm{diag}(e_1,\dots,e_n)$, respectively, where $a_i>0$, $b_i>0$, $c_i>0$, and $e_i>0$ for $i=1,\dots,n$. The following proposition discusses the sufficient conditions for matrix $\boldsymbol{W}$ to be negative semidefinite

Proposition 4. *$\boldsymbol{W}$ ($\boldsymbol{W}\in\mathbb{R}^{2n\times 2n}$) is a negative semidefinite matrix if matrices $\boldsymbol{D}_a$, $\boldsymbol{D}_b$, $\boldsymbol{D}_c$ and $\boldsymbol{D}_e$, and the discount parameter β are set such that*

$$a_i<\beta c_i,\forall i=1,2,\cdots,n \tag{46a}$$

$$e_i\ge\frac{-c_i^2}{\beta(a_i-\beta c_i)},\forall i=1,2,\cdots,n \tag{46b}$$

$$b_i\le\frac{c_i^2+\beta e_i(a_i-\beta c_i)}{a_i-\beta c_i},\forall i=1,2,\cdots,n \tag{46c}$$

for $\forall i$.

Proof. Matrix $\boldsymbol{W}$ can be expanded as

$$\begin{aligned}\boldsymbol{W}&=\left(\boldsymbol{A}-\frac{\beta}{2}\boldsymbol{E}_n\right)^{T}\boldsymbol{Q}_2+\boldsymbol{Q}_2\left(\boldsymbol{A}-\frac{\beta}{2}\boldsymbol{E}_n\right)+\boldsymbol{Q}_1\\&=\begin{bmatrix}\boldsymbol{0}_n & \boldsymbol{0}_n\\ -\boldsymbol{E}_n & \boldsymbol{0}_n\end{bmatrix}\begin{bmatrix}\boldsymbol{R}_4 & \\ & \boldsymbol{R}_5\end{bmatrix}+\begin{bmatrix}\boldsymbol{R}_4 & \\ & \boldsymbol{R}_5\end{bmatrix}\begin{bmatrix}\boldsymbol{0}_n & -\boldsymbol{E}_n\\ \boldsymbol{0}_n & \boldsymbol{0}_n\end{bmatrix}-\begin{bmatrix}\beta\boldsymbol{E}_n\boldsymbol{R}_4 & \\ & \beta\boldsymbol{E}_n\boldsymbol{R}_5\end{bmatrix}\\&\quad+\begin{bmatrix}\boldsymbol{R}_1 & \\ & \boldsymbol{R}_2\end{bmatrix}\\&=\begin{bmatrix}\boldsymbol{R}_1-\beta\boldsymbol{R}_4 & -\boldsymbol{R}_4\\ -\boldsymbol{R}_4 & \boldsymbol{R}_2-\beta\boldsymbol{R}_5\end{bmatrix}\end{aligned} \tag{47}$$

Denote $\widetilde{\boldsymbol{\Lambda}}=\begin{bmatrix}\boldsymbol{\Lambda} & \\ & \boldsymbol{\Lambda}\end{bmatrix}$, then

$$\begin{aligned}\widehat{\boldsymbol{W}}=\widetilde{\boldsymbol{\Lambda}}\boldsymbol{W}\widetilde{\boldsymbol{\Lambda}}^{T}&=\begin{bmatrix}\boldsymbol{\Lambda} & \\ & \boldsymbol{\Lambda}\end{bmatrix}\begin{bmatrix}\boldsymbol{R}_1-\beta\boldsymbol{R}_4 & -\boldsymbol{R}_4\\ -\boldsymbol{R}_4 & \boldsymbol{R}_2-\beta\boldsymbol{R}_5\end{bmatrix}\begin{bmatrix}\boldsymbol{\Lambda}^{T} & \\ & \boldsymbol{\Lambda}^{T}\end{bmatrix}\\&=\begin{bmatrix}\boldsymbol{\Lambda}(\boldsymbol{\Lambda}^{T}\boldsymbol{D}_a\boldsymbol{\Lambda}-\beta\boldsymbol{\Lambda}^{T}\boldsymbol{D}_c\boldsymbol{\Lambda})\boldsymbol{\Lambda}^{T} & -\boldsymbol{\Lambda}\boldsymbol{\Lambda}^{T}\boldsymbol{D}_c\boldsymbol{\Lambda}\boldsymbol{\Lambda}^{T}\\ -\boldsymbol{\Lambda}\boldsymbol{\Lambda}^{T}\boldsymbol{D}_c\boldsymbol{\Lambda}\boldsymbol{\Lambda}^{T} & \boldsymbol{\Lambda}(\boldsymbol{\Lambda}^{T}\boldsymbol{D}_b\boldsymbol{\Lambda}-\beta\boldsymbol{\Lambda}^{T}\boldsymbol{D}_e\boldsymbol{\Lambda})\boldsymbol{\Lambda}^{T}\end{bmatrix}\\&=\begin{bmatrix}\boldsymbol{D}_b-\beta\boldsymbol{D}_c & -\boldsymbol{D}_c\\ -\boldsymbol{D}_c & \boldsymbol{D}_b-\beta\boldsymbol{D}_e\end{bmatrix}\end{aligned} \tag{48}$$

According to Eq. (47), the eigenvalues of matrix $\widehat{\boldsymbol{W}}$ and $\boldsymbol{W}$ are identical. Let $\check{\boldsymbol{z}}_\beta=$

$\left(x_{1,\beta}, y_{1,\beta}, x_{2,\beta}, y_{2,\beta}, \ldots, x_{n,\beta}, y_{n,\beta}\right)^T$; $\check{\boldsymbol{z}}_\beta$ is a vector of variables obtained by changing the order of variables in $\boldsymbol{z}_\beta$. Then,

$$\left(\boldsymbol{z}_\beta\right)^T \widehat{\boldsymbol{W}} \cdot \boldsymbol{z}_\beta = \left(\check{\boldsymbol{z}}_\beta\right)^T \underbrace{\begin{bmatrix} \widetilde{\boldsymbol{W}}_1 & & & \\ & \widetilde{\boldsymbol{W}}_2 & & \\ & & \ddots & \\ & & & \widetilde{\boldsymbol{W}}_n \end{bmatrix}}_{\check{\boldsymbol{W}}} \cdot \check{\boldsymbol{z}}_\beta \tag{49}$$

where $\check{\boldsymbol{W}}$ is a block diagonal matrix defined above, in which $\widetilde{\boldsymbol{W}}_i$ $(\forall i = 1,2 \cdots, n)$ is

$$\widetilde{\boldsymbol{W}}_i = \begin{bmatrix} a_i - \beta c_i & -c_i \\ -c_i & b_i - \beta e_i \end{bmatrix} \tag{50}$$

Note $\widetilde{\boldsymbol{W}}_i$ is a symmetric matrix. It is negative semidefinite if

$$a_i - \beta c_i \leq 0 \tag{51a}$$

and

$$(a_i - \beta c_i)(b_i - \beta e_i) - c_i^2 \geq 0 \tag{51b}$$

Obviously, inequality (51a) holds if $a_i < \beta c_i$. According to Eq. (51b), we have

$$(a_i - \beta c_i)(b - \beta e_i) - c_i^2 = (a_i - \beta c_i) b_i - \beta e_i (a_i - \beta c_i) - c_i^2 \geq 0 \tag{52}$$

Note $a_i < \beta c_i$, inequality (52) implies that

$$b_i \leq \frac{c_i^2 + \beta e_i (a_i - \beta c_i)}{a_i - \beta c_i} \tag{53}$$

As $b_i \geq 0$, the right-hand side of inequality (53) holds only if

$$c_i^2 + \beta e_i (a_i - \beta c_i) \leq 0 \tag{54}$$

This implies

$$c_i^2 + \beta e_i (a_i - \beta c_i) \leq 0 \tag{55}$$

Thereby,

$$e_i \geq \frac{-c_i^2}{\beta (a_i - \beta c_i)} \tag{56}$$

The above discussion shows that if inequalities (53), (56), and $a_i < \beta c_i$ hold, $\widetilde{\boldsymbol{W}}_i$ is a negative semidefinite matrix. Similarly, we can infer that the block diagonal matrix $\check{\boldsymbol{W}}$ is negative semidefinite if inequalities (46a)-(46c) hold. This implies that $\widehat{\boldsymbol{W}}$ is negative semidefinite. Note that matrix $\widehat{\boldsymbol{W}}$ is similar to the symmetric matrix $\boldsymbol{W}$. Thereby, $\boldsymbol{W}$ is negative semidefinite if inequalities (46a)-(46c) hold. Proposition 4 is proved. ■

It is worth mentioning that Proposition 4 only provides a sufficient condition to ensure the asymptotic stability of the unconstrained idealized MPC strategy. There exist other conditions under which the unconstrained idealized MPC strategy is also asymptotically stable. Further, there may exists multiple equilibrium states for the CAV platoon depending on the speed of the leading vehicle. Proposition 4 only ensures the local stability the unconstrained idealized MPC strategy.

According to Proposition 4, the method to determine the diagonal positive definite matrices $\boldsymbol{D}_a$, $\boldsymbol{D}_b$, $\boldsymbol{D}_c$ and $\boldsymbol{D}_e$ and the discount parameter β to ensure asymptotic stable of the unconstrained idealized MPC strategy can be summarized as follows. First, set an arbitrary positive value for β and a diagonal positive definite matrix $\boldsymbol{D}_c$. Second, obtain the matrix $\boldsymbol{D}_a$ such that inequality (56a) is satisfied. Then, obtain matrices $\boldsymbol{D}_e$ and $\boldsymbol{D}_b$ according to inequalities (56b) and (56c), respectively.

6. Numerical experiments

This section discusses four numerical experiments to demonstrate the motivation for this study and to illustrate the effectiveness of the proposed DMPC-FOA approach. The first numerical experiment analyzes the computational time required for the leading vehicle to solve optimal control problem (5) for different initial inputs, prediction horizons, and the number of following vehicles. The second numerical experiment illustrates the detailed steps for sensitivity analysis of the optimal control problem. The first-order Taylor approximation method is then applied to estimate the solution of state variables, costate variables, and the optimal control decisions when the leading vehicle's initial speed and position are changed. The estimated solution and the exact solution (computed using the solution algorithm in Section 3) are compared. The third numerical experiment compares the control performance of the DMPC-FOA approach with that of the DMPC approach assuming the movement of the leading vehicle is predetermined according to NGSIM field data. The fourth numerical experiment shows a traffic flow scenario where the DMPC approach fails to control the CAV platoon safely due to poor estimation of the optimal control decisions of the idealized MPC strategy. However, the DMPC-FOA approach can control the CAV platoon effectively and is able to characterize the optimal control decisions of the idealized MPC strategy accurately in this scenario. The last numerical experiment apply two more scenarios to test the performance of the proposed DMPC-FOA approach.

6.1 Computational time for solving optimal control problem (5)

The DMPC approach and DMPC-FOA approach need to reserve τ_1 and τ_2 time before each time instant, respectively, to estimate the optimal control decisions of the idealized MPC approach. τ_1 should be large enough such that the optimal control problem (5) (i.e., the two-point boundary value problem (32)) can be solved using the shooting method, while τ_2 should be sufficiently large so as to solve the two-point boundary value problems (32), (35) and (37) with the shooting method. Note that the computational times for the two-point boundary value problems significantly depend on the platoon size (n), the prediction horizon (T_P) and the initial state of the CAV platoon. In this study, the values of τ_1 and τ_2 will be determined offline according to platoon size and the prediction horizon. For each platoon size (varying from 2 to 15) and the prediction horizon (varying from 1 second to 8 seconds), we randomly generated 1000 initial states of the CAV platoon. The shooting method is applied to solve the two-point boundary value problems (32), (35) and (37) under each initial state. The computational time for solving the two-point boundary value problems (32) corresponding to 0.95 cumulative probability is used as the baseline for τ_1, while the total computational time for solving the two-point boundary value problems (32), (35) and (37) corresponding to 0.95 cumulative probability is used as the baseline for τ_2.

Table 1 shows the detailed inputs of the parameters in the optimal control problem (5). These inputs are used for all four numerical experiments. The discount parameter β and the matrices $\boldsymbol{R}_1$, $\boldsymbol{R}_2$, $\boldsymbol{R}_4$, and $\boldsymbol{R}_5$ in optimal control problem (5) are set as follows: $\beta = 1$, $\boldsymbol{R}_1 = 0.5\boldsymbol{E}_n$, $\boldsymbol{R}_2 = \boldsymbol{R}_4 = \boldsymbol{E}_n$, $\boldsymbol{R}_5 = 3\boldsymbol{E}_n$. These inputs satisfy the inequalities in Proposition 4 to ensure that the unconstrained idealized MPC strategy is asymptotic stable. It is worth mentioning that the value of β decides the weights of the running cost at different time in future. It not only impacts the stability of the benchmark MPC approach, but also the estimation performance of the DMPC-FOA approach. Our analysis shows that the stability

performance of the benchmark MPC approach and the estimation performance of the DMPC-FOA are better when $\beta \in [0.5,1.5]$.

Table 1. Input parameters for optimal control problem (5)

Variables	Default value
Minimum acceleration (u_{min})	$-5\ m/s^2$
Maximum acceleration (u_{max})	$3\ m/s^2$
Minimum spacing (s_{min})	$5\ m$
Safety space (s_f)	$10\ m$
Speed limit (v_{max})	$33.5\ m/s\ (120\ km/h)$
Time headway (r^*)	$1\ s$

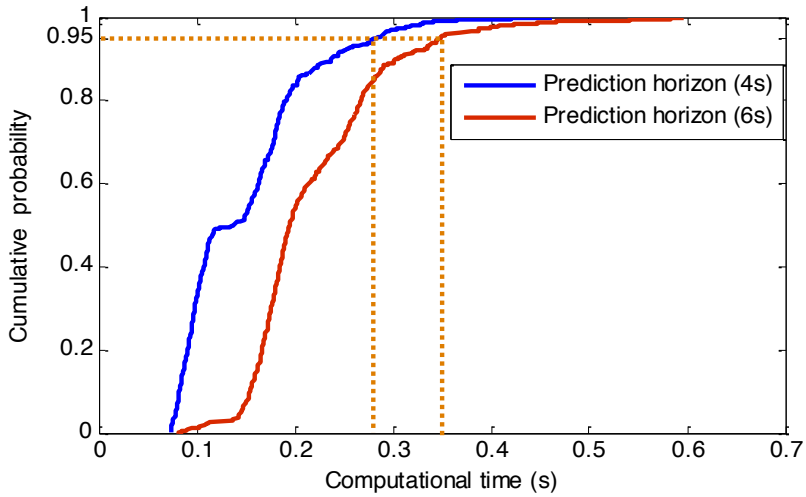

Fig. 5. Cumulative probability of computational time for solving optimal control problem (5) with different initial inputs (i.e., $\mathbf{x}(0)$ and $\mathbf{y}(0)$) at $n = 8$ and $T_P = 4s$ and $6s$.

Without loss of generality, suppose the initial time is 0. To ensure that optimal control problem (5) can be solved within τ_1 seconds under different initial inputs of position errors (i.e., $\mathbf{x}(0)$) and speed differences (i.e., $\mathbf{y}(0)$) of all adjacent vehicles pairs, $\mathbf{x}(0)$ is generated randomly in the interval $[-10,100]$ and $\mathbf{y}(0)$ is randomly generated in the interval $[0,20]$. This study generates 1000 different values for $\mathbf{x}(0)$ and $\mathbf{y}(0)$ for which the inequality constraints (Eq. (5c)) are satisfied.

The numerical experiments were coded in MATLAB and executed on a computer with an Intel Core i7-4790 3.60-GHz CPU with 8.00 GB of RAM. To analyze the impacts of the number of following vehicles in the platoon (n) and the prediction horizon (T_P) on computational time, optimal control problem (5) is solved 1000 times under different feasible initial inputs for each combination of n and T_P.

Fig. 5 shows the cumulative probability of computational time for solving the optimal control problem (5) with different initial inputs (i.e., $\mathbf{x}(0)$ and $\mathbf{y}(0)$) for $n = 8$ and $T_P = 4s$ and $6s$. It shows that the computational time significantly depends on the value of $\mathbf{x}(0)$ and $\mathbf{y}(0)$. The computational time ranges from 0.08s to 0.4s under $n = 8$ and $T_P = 4s$. It is worth noting that computational times are large only when the initial position errors of many adjacent vehicle pairs deviate remarkably from the equilibrium state (i.e., they are close to 100 m), the likelihood of occurrence of which is low in the real

world. Hence, this study uses the computational time corresponding to 0.95 cumulative probability as the reference point to determine the reserved time for the DMPC and DMPC-FOA approaches.

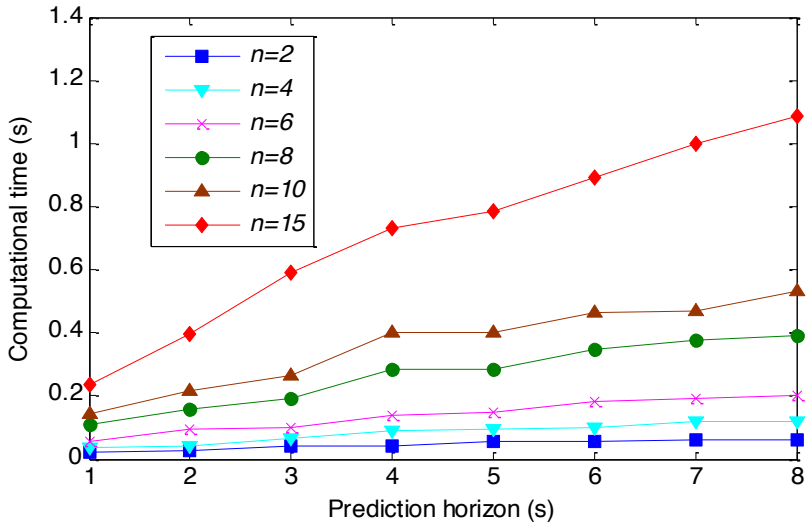

Fig. 6. Computational time corresponding to 0.95 cumulative probability under different n and T_P.

Fig. 6 shows the computational time corresponding to 0.95 cumulative probability under different n and T_P. The computational time corresponding to 0.95 cumulative probability is the time within which 95% of the experimental scenarios can be solved. Fig. 6 illustrates that the computational time corresponding to 0.95 cumulative probability increases monotonically with the number of following vehicles and the prediction horizon.

6.2 Sensitivity analysis of optimal control problem (5)

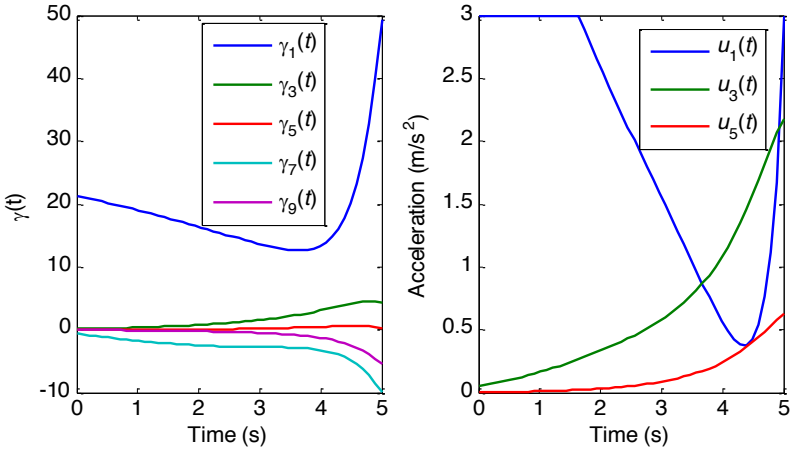

(a) (b)

Fig. 7. Solutions of costate variables and optimal control decisions at the unperturbed initial state: (a) solutions of costate variables; (b) optimal control decisions.

This section shows the details of the sensitivity analysis method implementation for the optimal control problem (5) introduced in section 4. Consider a CAV platoon with 5 following vehicles ($n = 5$). The leading vehicle and all following vehicles drive at a speed of 20 m/s at time 0 (i.e., $\mathbf{y}(0) = 0$). Suppose the initial position errors of vehicle 2 to vehicle 5 are all 0, and the initial position error of vehicle 1 with

respect to the leading vehicle is 90 m. This implies that the spacing between vehicle 1 and vehicle 0 is $90 + T \cdot 20 + s_f = 120m$. It indicates a case where the following vehicles seek to catch up with the leading vehicle. Let $T_P = 5\ s$. Fig. 7(a) shows the optimal solutions of the costate variables obtained using the solution algorithm proposed in Section 3. The optimal control decisions of all following vehicles in the platoon can then be determined according to Eq. (23). Fig. 7(b) shows the optimal control decisions of vehicles 1, 3 and 5. It indicates that vehicle 1 accelerates at the maximum value ($3\ m/s^2$) for the first 1.7 seconds. Then, the acceleration decreases monotonically in the time interval $[1.7\text{s}, 4.3\text{s}]$ and then increases.

Suppose the initial position and speed of the leading vehicle at time 0 are perturbed. Then, $x_1(0)$ and $y_1(0)$ change from the unperturbed values 90 and 0, respectively. Fig. 8 shows the derivatives of solutions for the state and costate variables with respect to $x_1(0)$ and $y_1(0)$, respectively. They are obtained by solving the two-point boundary value problem (35) and (37), respectively. Fig. 8 shows that at the optimal state, a unit change in $x_1(0)$ and $y_1(0)$ will increase the optimal solution of $x_1(t)$ and $y_1(t)$ by 1, respectively, at time interval $[0,1.7]$. The impacts of variations in $x_1(0)$ and $y_1(0)$ on $x_1(t)$ and $y_1(t)$ decrease after 1.7 seconds.

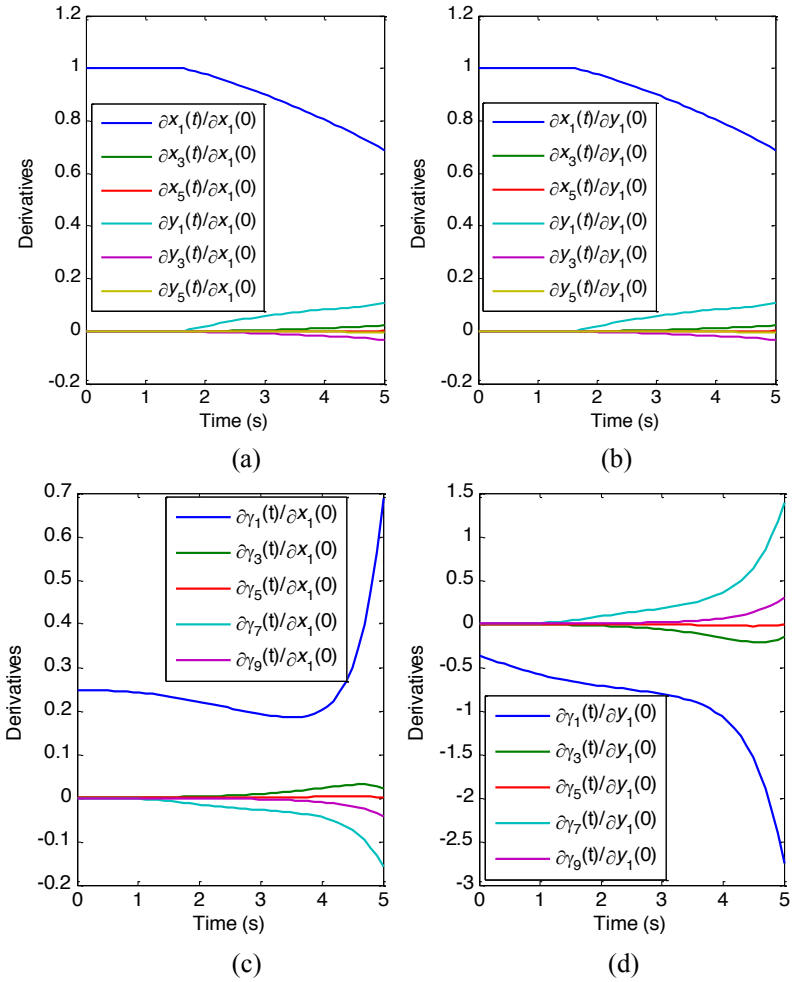

Fig. 8. Derivatives of the state and costate variables with respect to $x_1(0)$ and $y_1(0)$, respectively, at the unperturbed initial state: (a) derivatives of the state variables with respect to $x_1(0)$; (b) derivatives of the state variables with respect to $y_1(0)$; (c) derivatives of the costate variables with respect to $x_1(0)$; (d) derivatives of the costate variables with respect to $y_1(0)$.

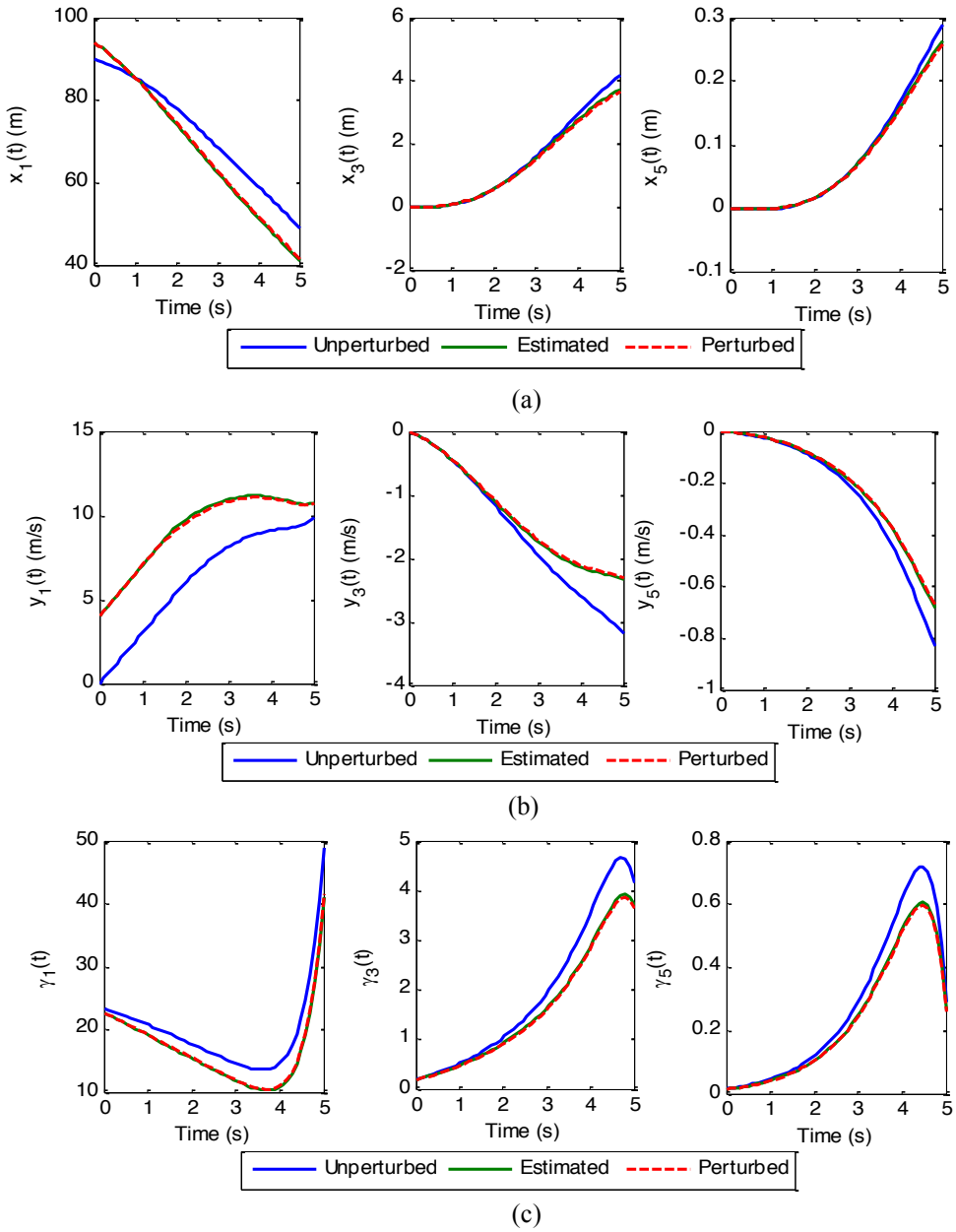

Fig. 9. Comparison of estimated and perturbed optimal solutions for the state and costate variables: (a) comparison of estimated and perturbed optimal solutions of position errors; (b) comparison of estimated and perturbed optimal solutions of speed difference for adjacent vehicle pairs; (c) comparison of estimated and perturbed optimal solutions for the costate variables.

Suppose both $x_1(0)$ and $y_1(0)$ are increased by 4 units (for example, due to prediction error). Using the first-order Taylor approximation (Eq. (38)), Fig. 9 compares the estimated and perturbed optimal solutions for the state variables and costate variables. The perturbed solutions are obtained using the solution algorithm at the perturbed states of $x_1(0)$ and $y_1(0)$. Fig. 9 shows that the estimated solutions are very close to those of the perturbed solutions, indicating that the first-order Taylor approximation can accurately characterize the variation in the optimal solutions induced by changes in $x_1(0)$ and $y_1(0)$. Based on the estimated solutions for the costate variables (i.e., $\boldsymbol{\gamma}$), Fig. 10 compares the optimal control decisions of following vehicles estimated by Eq. (39) and the perturbed ones obtained using the solution

algorithm in Section 3. It shows that the estimated solutions are also very close to the perturbed ones obtained using the solution algorithm.

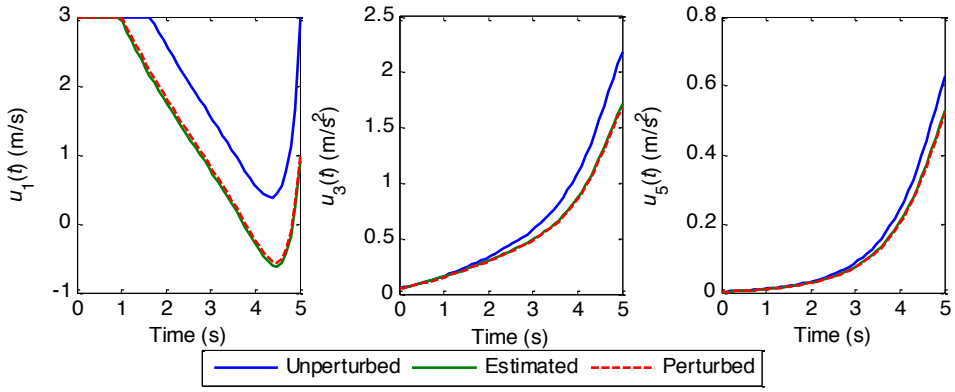

Fig. 10. Comparison of estimated and perturbed optimal control decisions of the following vehicles.

6.3 Control performance of the DMPC and DMPC-FOA approaches

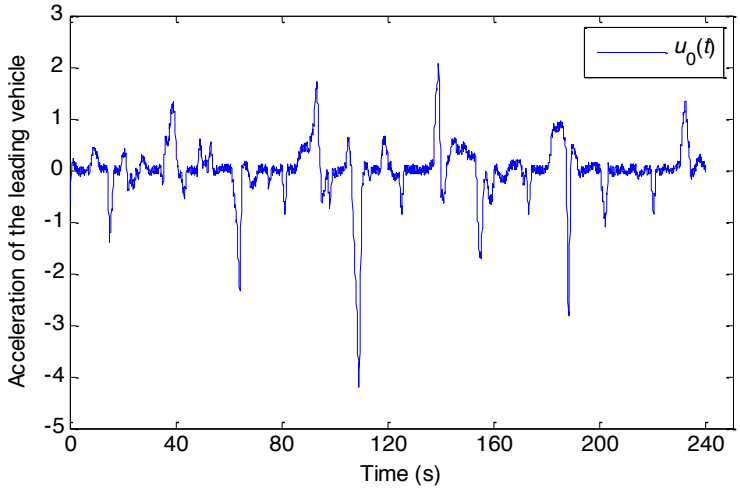

Fig. 11. Acceleration of the leading vehicle

Note that both the DMPC and DMPC-FOA approaches seek to address the issue of control delay and estimate the optimal control decisions of the idealized MPC strategy. This section compares the control decisions of the DMPC approach, the DMPC-FOA approach and the idealized MPC strategy. To do so, we consider a CAV platoon with 8 following vehicles (vehicle IDs 1-8). The acceleration of the leading vehicle is shown in Fig. 11. It contains a 240-seconds (with resolution 0.1 second) real-world vehicle control diary collected on eastbound I-80 in the San Francisco Bay area at Emeryville, California. It can be noted that the vehicle decelerated or accelerated mildly most of the time. However, it contains some time slots with hard braking and high acceleration (e.g., the time slots around 110s, 140s and 186s).

Suppose the prediction horizon and the roll period are $T_P = 5$ seconds and $\Delta t = 1$ second, respectively. According to Fig. 6, the computational time for solving optimal control problem (5) corresponding to 95% cumulative probability with 8 following vehicles is 0.33 seconds. To reserve enough time for solving the optimal control problem, τ_1 is set as 0.4 seconds for the DMPC approach. Note that the DMPC-FOA approach needs to solve optimal control problem (5) as well as perform sensitivity analysis of the optimal control problem with respect to $\tilde{x}_1(0)$ and $\tilde{y}_1(0)$. Thereby, $\tau_2 \geq \tau_1$.

From 1000 simulations, the total computational time for solving the optimal control problem (5) and the two-point boundary value problems (problems (35) and (37)) corresponding to 95% cumulative probability is around 0.56 seconds. Thereby, τ_2 is set as 0.6 seconds. It should be noted that among the 1000 simulations, there are situations where some following vehicles need to brake and accelerate at the maximum rate during the prediction horizon. Thereby, $\tau_2 = 0.6s > \tau_1 = 0.4s$. According to Proposition 3, if these situations do not exist and the spacing of each following vehicle is always greater than the minimum value (s_{min}), τ_2 can be set the same as τ_1.

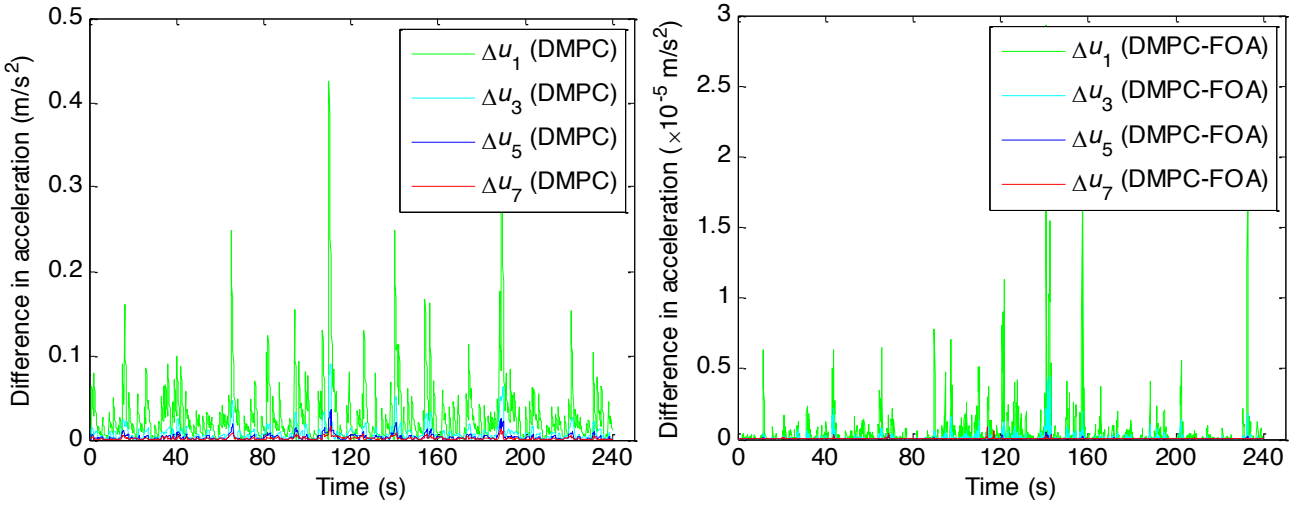

(a) (b)

Fig. 12. Differences between the estimated control decisions of the DMPC and DMPC-FOA approaches from those of the idealized MPC strategy: (a) difference between control decisions of the DMPC approach and those of the idealized MPC strategy; (b) difference between control decisions of the DMPC-FOA approach and those of the idealized MPC strategy.

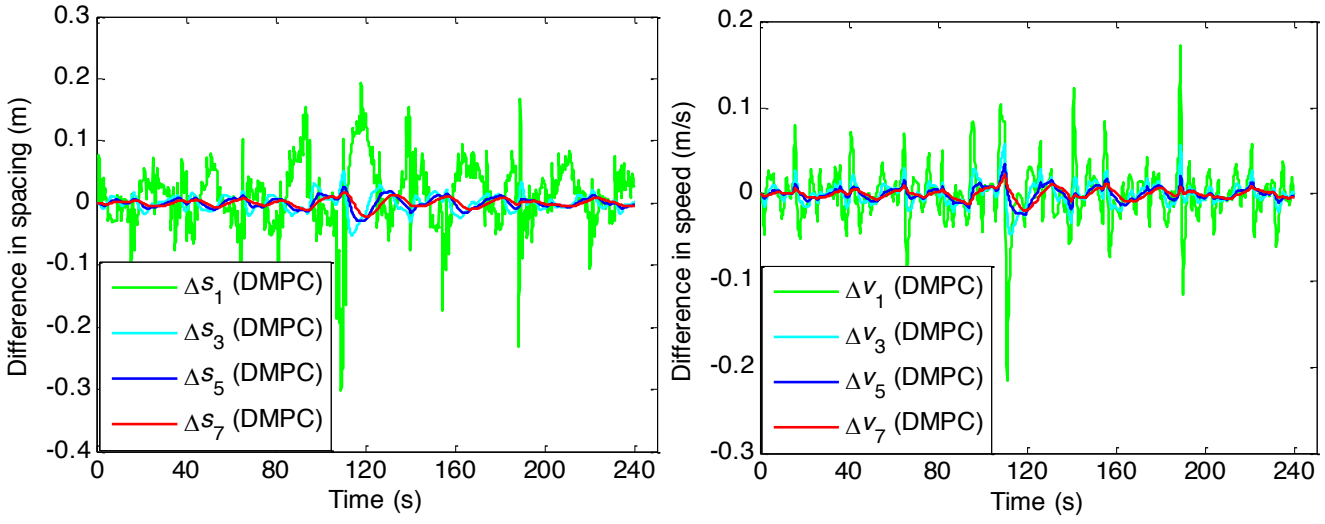

(a) (b)

Fig. 13. Differences in optimal spacing and speed between the DMPC approach and the idealized MPC strategy: (a) difference in optimal spacing; (b) difference in optimal speed.

Fig. 12 shows the difference between the estimated control decisions of the DMPC approach (i.e, $\Delta u_i = \hat{u}_i^*(t) - u_i^*(t), \forall i = 1,2,\cdots n$) and the DMPC-FOA approach (i.e, $\Delta u_i = \bar{u}_i^*(t) - u_i^*(t), \forall i = 1,2,\cdots n$) from those of the idealized MPC strategy. Fig. (12a) shows that the estimated control decisions

of the DMPC approach are close to those of the idealized MPC strategy with the maximum difference less than 0.45 m/s^2. The estimation errors of the control decisions of DMPC approach are induced by the prediction error of $x_1(t)$ and $y_1(t)$ at each sampling time instant. However, through first-order Taylor's approximation, the DMPC-FOA approach can significantly improve on the estimation performance of the DMPC approach. As can be seen from Fig. 12(b), the maximum difference between the control decisions estimated by the DMPC-FOA approach and the idealized MPC strategy is less than $3 \times 10^{-5}\ m/s^2$, indicating that the DMPC-FOA approach can characterize the decisions of the idealized MPC strategy very well.

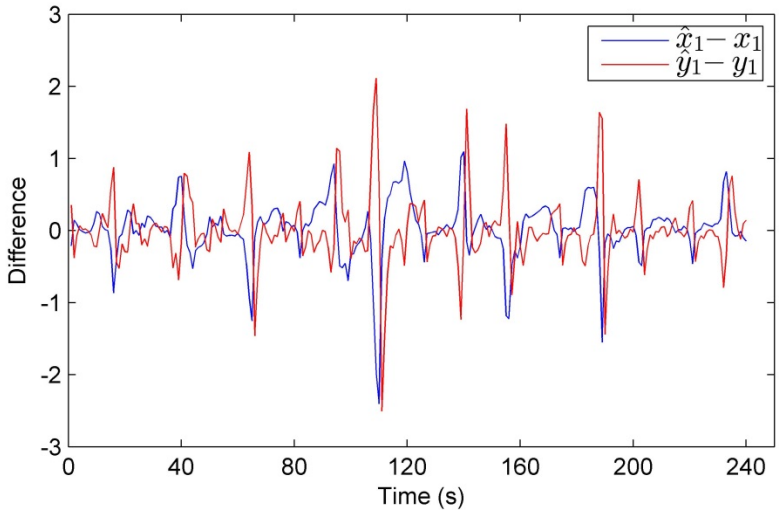

Fig. 14. Prediction errors of the initial states of $x_1(t_k)$ and $y_1(t_k)$, $t_k = 1s, 2s, \cdots, 240s$.

Fig. 13 illustrates the differences in optimal spacing and speed between the DMPC approach and the idealized MPC (i.e., Δs_i and Δv_i, respectively, $i = 1,2, \cdots n$). It shows that while the estimated control decisions of DMPC approach deviate from the idealized MPC strategy, the optimal spacing and speed obtained by the DMPC approach are very close to those of the idealized MPC strategy. Hence, the DMPC approach is able to control the CAV platoon efficiently in this case. To investigate the reason for the good control performance of the DMPC approach in this scenario, Fig. 14 shows the prediction errors of the initial inputs of $x_1(t)$ and $y_1(t)$ at each sampling time instant $t_k, k = 1,2, \cdots$. Recall $\Delta t = 1s$. Hence, $t_k = 1s, 2s, \cdots, 240s$. It shows that the predicted values of $x_1(t_k)$ and $y_1(t_k), k = 1,2, \cdots$ are very close to those of the exact ones as the leading vehicle drives with mild acceleration or deceleration most of the time (see Fig. 11). The large prediction error occurs at the moments when the leading vehicle has hard acceleration or deceleration (e.g., $t = 110s, 140s, 186s$ etc.). Correspondingly, the DMPC approach also has larger estimation errors in terms of the optimal solutions relative to those of the idealized MPC strategy (see Fig. 12(a) and Fig. 13). However, as these "extreme" behaviors of the leading vehicle only last for small time periods, their impacts are small. In addition, if $x_1(t_k)$ and $y_1(t_k)$ are accurately predicted at a time instant t_k, the large difference in optimal solutions between the DMPC approach and the idealized MPC strategy in the previous roll period will be reduced significantly at the current roll period starting from time instant t_k. This can be observed in Fig. 12(a) and Fig. 13 where the large differences at time instants $t = 110s, 140s, 186s$ are reduced dramatically in the roll periods following time instants at which $x_1(t)$ and $y_1(t)$ are predicted with low errors at the corresponding sampling time instants (i.e., $t_k = 111s, 141s, 187s$, see Fig. 14).

Fig. 15 shows the control decisions of the following vehicles estimated by the DMPC-FOA approach. It indicates that when the leading vehicle 0 executes hard acceleration/deceleration, vehicle 1 also executes hard acceleration/deceleration with a magnitude slightly less than that of the leading vehicle 0. The acceleration or deceleration decreases sequentially in the platoon, indicating that the traffic oscillation is damped sequentially from the head of the platoon to its tail. Fig. 16 shows the optimal spacing and speed differences of adjacent vehicle pairs in the platoon computed by the DMPC-FOA approach. These results are almost identical to those of the idealized MPC strategy with the maximum absolute error less than 8×10^{-8} due to the high accuracy of the estimated optimal control decisions (see Fig. 12(b)). As can be seen in Fig. 16, the oscillation of the optimal spacing and speed difference of adjacent vehicle pairs decreases sequentially in the platoon. These results indicate that the DMPC-FOA approach can lead to smooth deceleration and acceleration behavior of all following vehicles. In addition, it can coordinate the behavior of all following vehicles to dissipate the traffic oscillation to ensure stability of the CAV platoon.

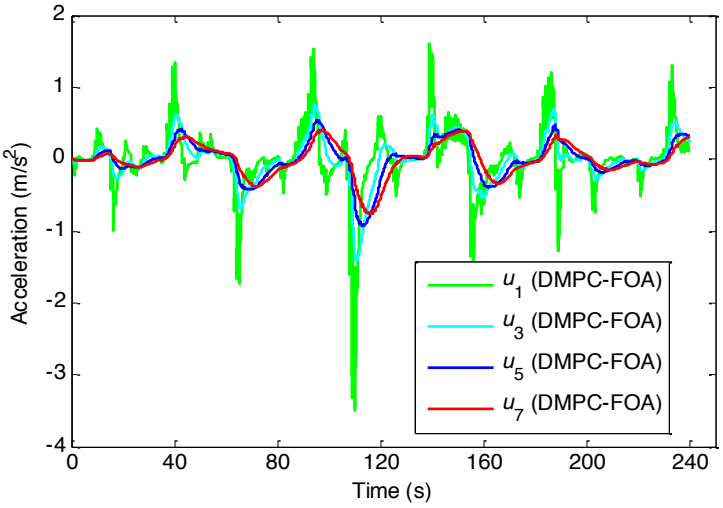

Fig. 15. Estimated control decisions of the DMPC-FOA approach.

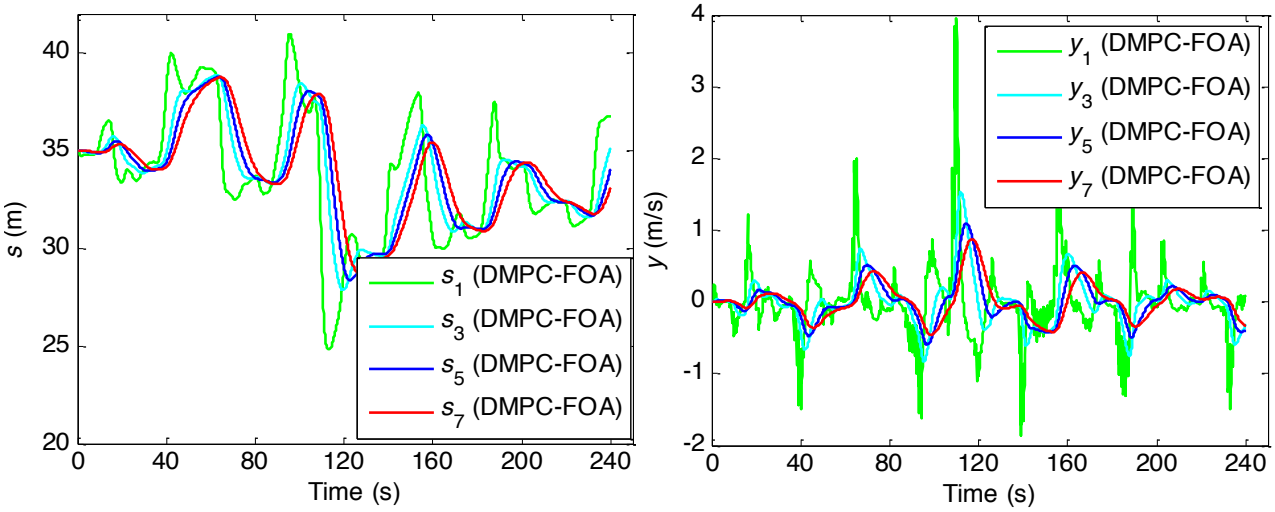

(a) (b)

Fig. 16. Optimal spacing and speed difference for some adjacent vehicle pairs in the platoon computed by DMPC-FOA approach: (a) spacing of adjacent vehicle pairs; (b) speed difference of adjacent vehicle pairs.

6.4 Scenario where the DMPC approach fails to control the CAV platoon

The previous section illustrated a scenario in which the estimated control decisions and the solutions for the state variables of the DMPC approach are very close to those of the idealized MPC strategy. Here, we illustrate a scenario in which when the DMPC approach fails to accurately predict the values of $x_1(t_k)$ and $y_1(t_k)$ at each sampling time instant t_k, the error of the control decisions between the DMPC approach and idealized MPC strategy increases with each roll period. Then, the car-following behavior of the vehicles controlled by the DMPC approach significantly deviates from that of the idealized MPC strategy. However, as will be illustrated, the DMPC-FOA approach accurately characterizes the optimal control decisions of the idealized MPC strategy.

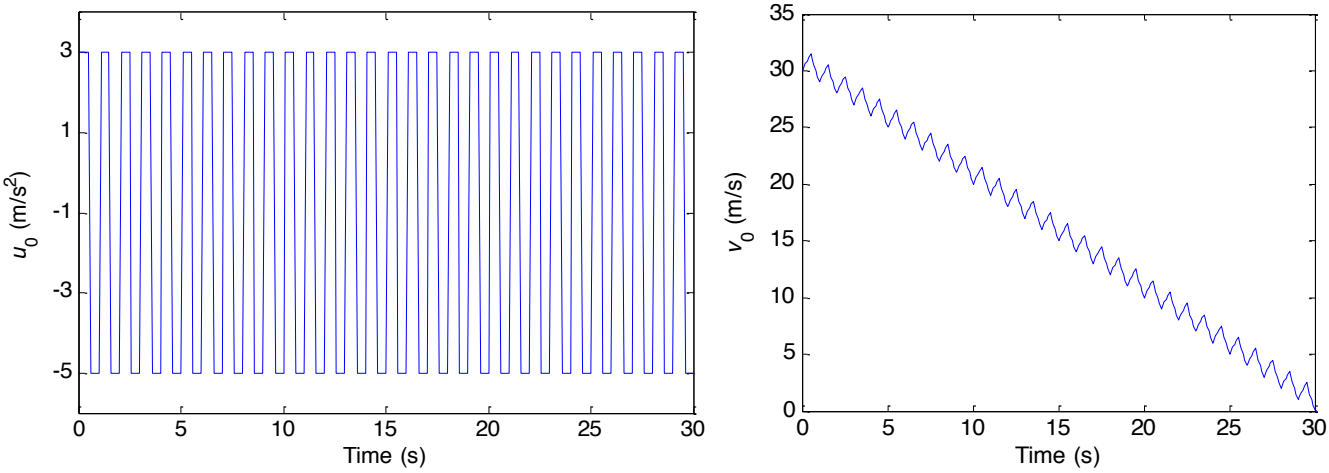

(a) (b)

Fig. 17. Acceleration and speed of the leading vehicle: (a) acceleration of the leading vehicle; (b) speed of the leading vehicle.

Consider a CAV platoon with 10 following vehicles. Let $T_P = 5$ seconds and $\Delta t = 1$ second. According to Fig. 6, the computational time corresponding to 95% cumulative probability is 0.42 seconds. Hence, we set $\tau_1 = 0.5$ seconds for the DMPC approach. By conducting 1000 simulation runs with different initial inputs for $x_1(0)$ and $y_1(0)$, the computational time corresponding to 95% cumulative probability for the DMPC-FOA approach is determined as 0.66 seconds. We will set $\tau_2 = 0.7$ seconds for the DMPC-FOA approach.

Suppose the leading vehicle drives at 30 m/s at time 0. Assume the leading vehicle accelerates at the maximum value 3 m/s^2 for 0.5 seconds and then decelerates at the maximum value -5 m/s^2 for 0.5 seconds. Such behavior will repeat for 30 seconds until the leading vehicle stops. Fig. 17(a) shows the trajectory of the assumed acceleration of the leading vehicle. The corresponding speed of the leading vehicle is shown in Fig. 17(b).

As $\Delta t = 1$ second, the sampling time instant $t_k = k$ seconds for $k = 1,2,\cdots$. Under the assumed acceleration behavior of the leading vehicle, the prediction errors of $x_1(t_k)$ and $y_1(t_k)$ using the DMPC approach are -1 m and 4 m/s, respectively, at each sampling time instant t_k. Note that the prediction errors of $x_1(t_k)$ and $y_1(t_k)$ $(k = 1,2,3\cdots)$ for DMPC-FOA are the same as that of DMPC approach.

Fig. 18 compares the optimal solutions for the DMPC approach, the DMPC-FOA approach and the idealized MPC strategy. It illustrates that both spacing and control decisions of vehicle 1 computed using

the DMPC approach deviate significantly from those of the idealized MPC strategy due to the large prediction errors of $x_1(t_k)$ and $y_1(t_k)$ $(k = 1,2,\cdots)$. In addition, the spacing between the leading vehicle 0 and vehicle 1 even reduce to a value less than the minimum allowable spacing $s_{min}(s_{min} = 5\ m)$. Thereby, a collision will occur between leading vehicle 0 and vehicle 1 in the platoon. Note that the DMPC approach stops at $t = 18s$ as the safety constraints (inequality (5c)) cannot be satisfied thereafter. Hence, no solution can be found using the DMPC approach. By contrast, the DMPC-FOA approach provides an optimal solution very close to that of the idealized MPC strategy. When the leading vehicle stops at $t = 30s$, the spacing between leading vehicle 0 and vehicle 1 is over $10\ m$ to ensure safety. These results highlight that the DMPC-FOA approach can effectively improve the estimation performance significantly beyond that of the DMPC approach even under extreme scenarios.

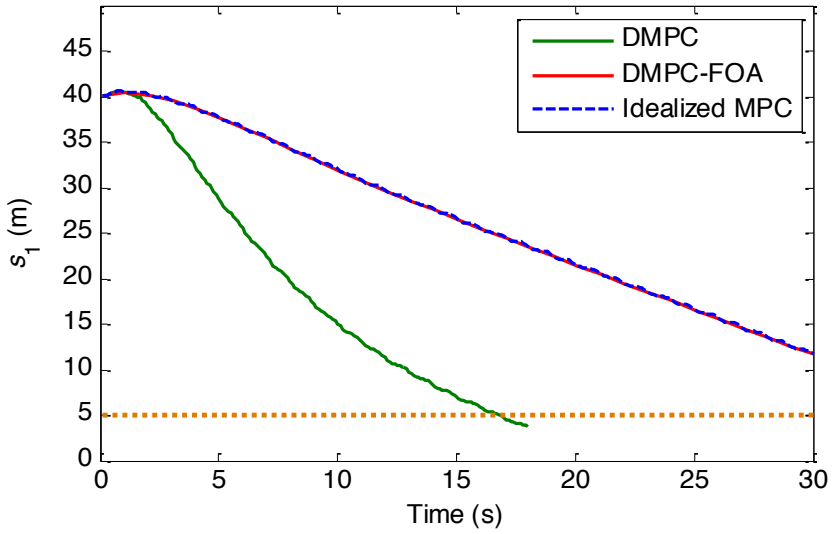

(a)

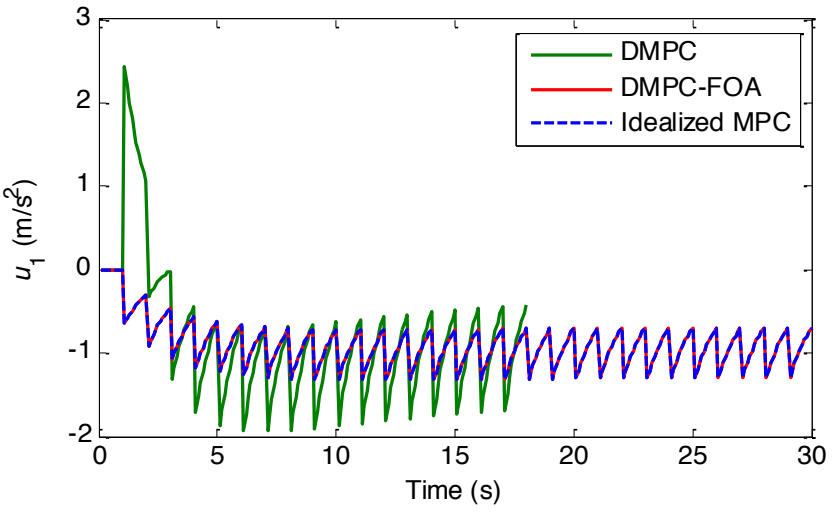

(b)

Fig. 18. Comparison of solutions for spacing and control decisions of vehicle 1 among the DMPC approach, the DMPC-FOA approach and the idealized MPC strategy: (a) comparison of solution for spacing of vehicle 1; (b) comparison of control decisions for vehicle 1

The control performances of the above two scenarios show that when the leading vehicle decelerates or accelerates mildly and less frequently (e.g., when traffic density is low), the DMPC approach is

sufficient to control the CAV platoon efficiently. However, when the leading vehicle executes a hard brake or accelerates frequently (e.g., in congested traffic flow), the DMPC-FOA approach should be applied to ensure the safety and efficiency of the CAV platoon.

6.5 Two other scenarios to test the control performances of DMPC-FOA approach

In this section, the following two traffic scenarios are considered to validate the performance of the DMPC-FOA approach. Assume that the number of following CAVs in the platoon is 8. Let $\tau_2 = 0.6$ seconds.

In scenario 1, the leading vehicle performs acceleration and deceleration maneuvers to represent a situation in which the platoon approaches a traffic jam on a highway and moves out of the traffic jam afterwards. In the simulation of 180 seconds, the leading vehicle drives at a constant speed of 25 m/s for 20 seconds. It decelerates at -4 m/s^2 and accelerates at 3 m/s^2 in time $[20s, 23s]$ and $[110s, 114s]$, respectively.

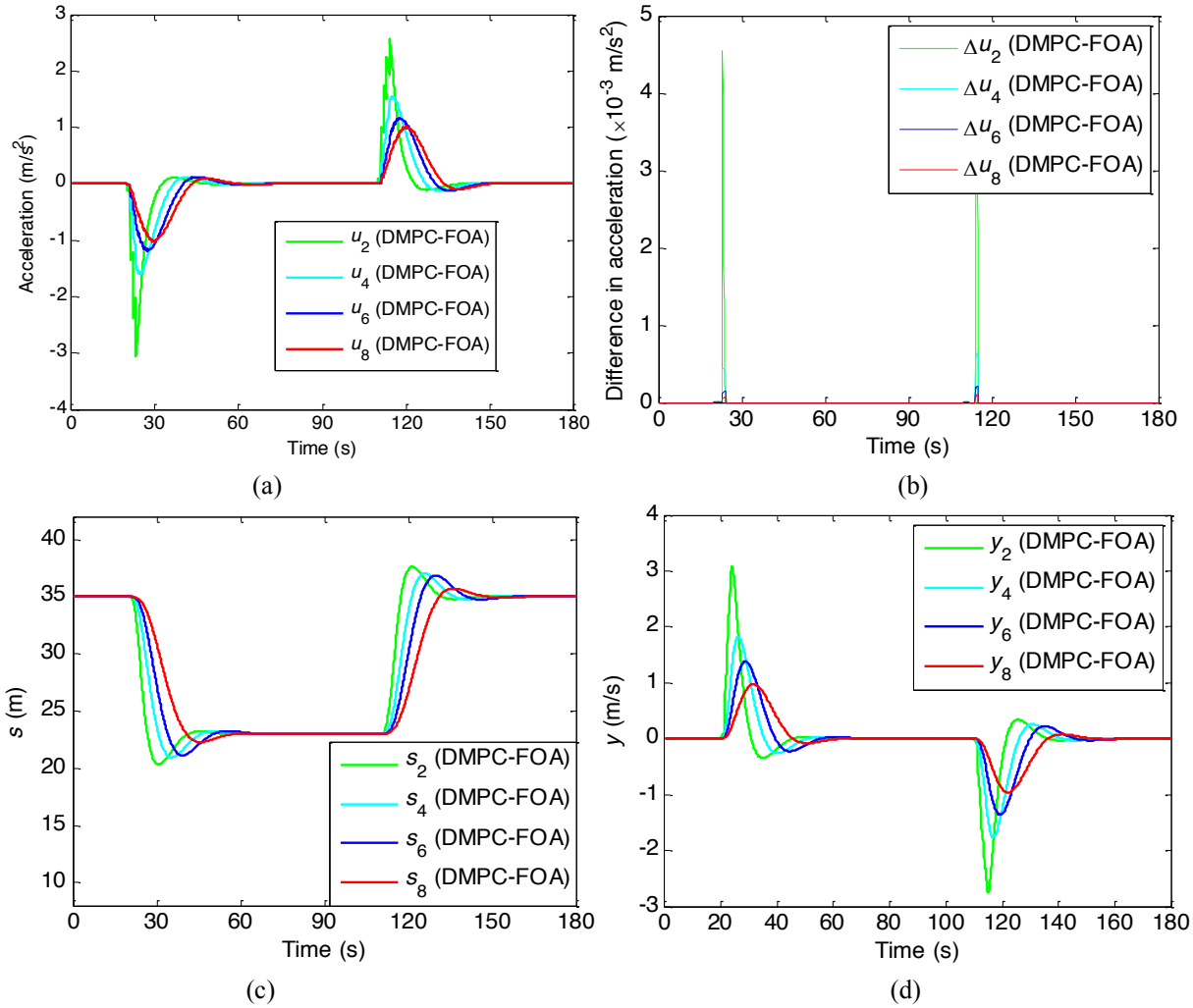

Fig 19. Optimal results computed by DMPC-FOA approach for scenario 1: (a) Control decision; (b) Difference in optimal control decisions between the DMPC approach and the idealized MPC strategy; (c) spacing of adjacent vehicle pairs; (d) difference in speed of adjacent vehicle pairs

In scenario 2, suppose the platoon approaches a signalized intersection. The leading vehicle drives

at a constant speed of 30 m/s initially and decelerates at -2 m/s^2 at $t = 10$s until it stops completely.

Figure 19 shows the optimal results of the DMPC-FOA approach for scenario 1. As can be seen, the magnitudes of deceleration and acceleration decrease from the head of the platoon to its tail, implying that the scale of perturbation decreases sequentially in the platoon (Figure 19(a)). Figure 19(b) shows that the maximum error of the estimated optimal control is less than 5×10^{-3} m/s^2, indicating that the DMPC-FOA approach can accurately characterize the optimal control of the idealized MPC approach. Figure 19(c) and Figure 19(d) illustrate the evolution of space headway and speed difference of adjacent vehicle pairs, respectively. These results further validate that the DMPC-FOA approach can damp traffic oscillations effectively.

For scenario 2, similarly, the DMPC-FOA approach can accurately estimate the optimal control decisions of the idealized MPC approach (see Figure 20(a)). The following vehicles decelerate when the leading vehicle decelerates and converge to the equilibrium state sequentially (see Figure 19(b)). The evolution of space headway and speed difference of adjacent vehicle pairs show that the traffic oscillation decays in the platoon (Figures 20(c) and 20 (d)). ”

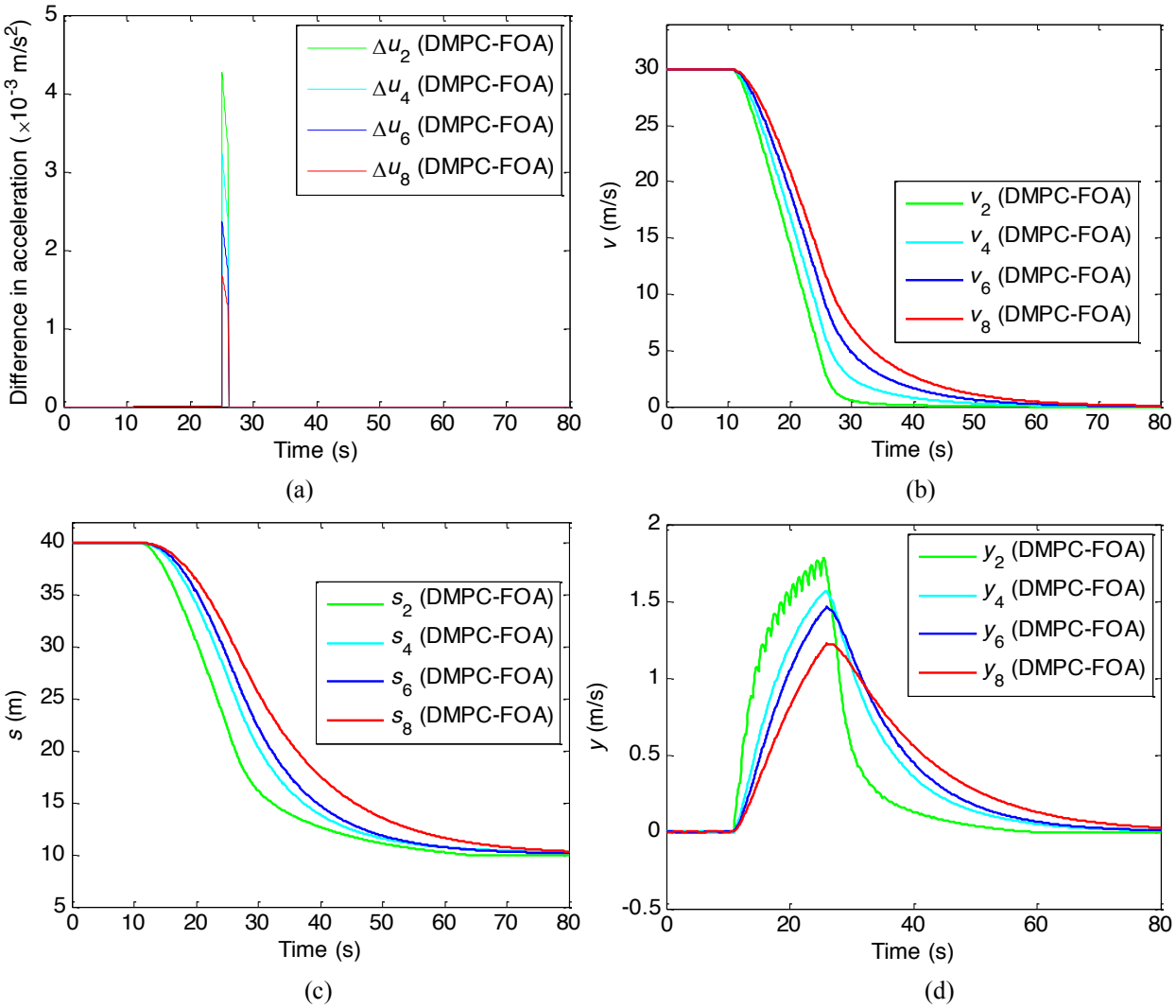

Fig 20. Optimal results computed by DMPC-FOA approach for scenario 2: (a) Difference in optimal control decisions between the DMPC approach and the idealized MPC strategy; (2) speed of each vehicle; (c) spacing of adjacent vehicle pairs; (d) difference of speed of adjacent vehicle pairs.

7. Concluding comments

This study first proposes an idealized MPC-based cooperative control strategy for CAV platooning. Its optimal control decisions can coordinate the behaviors of all following CAVs in the platoon to maneuver them effectively and safely. However, as in existing literature, it is based on the idealized, but unrealistic, assumption that the embedded optimal control problem can be solved instantaneously. To relax this idealized assumption, two deployable strategies, i.e., the DMPC approach and the DMPC-FOA approach, are proposed to address the control delay issue of the idealized MPC strategy and to accurately characterize its optimal control decisions. The DMPC approach addresses the control delay issue by reserving sufficient time before each sampling time instant to solve the embedded optimal control problem. However, the estimated control decisions of the DMPC approach can deviate significantly from those of the idealized MPC strategy due to errors in predicting the leading vehicle's position and speed. By contrast, the DMPC-FOA approach addresses the control delay issue effectively while accurately characterizing the optimal control decisions of the idealized MPC strategy by leveraging the proposed analytical sensitivity analysis method for the embedded optimal control problem. The application of the DMPC-FOA approach for a CAV platoon whose lead vehicle's trajectory is obtained from field data illustrates that it can dampen traffic oscillations efficiently, and can enable smooth deceleration and acceleration behaviors for all following vehicles. In addition, it can provide control decisions very similar to those of the idealized MPC strategy even under extreme situations where the leading vehicle's speed and position are predicted very poorly at each sampling time instant.

It is important to note that the DMPC-FOA approach concept can also be leveraged to address the issue of control delay for other MPC-based cooperative control strategies (e.g., Wang et al., 2014b) arising from the computational time required to solve the embedded optimal control problem. It can be applied for real-time control of large CAV platoons on the condition that the time reserved for computing (i.e., τ_2) is less than the roll period (Δt).

It should be noted that while the proposed DMPC-FOA approach can fundamentally address the control delay issue induced by the computational time for the optimal control problem, there is the need to relax some assumptions in this study to make the control approach more robust and reliable to deal with real-world situations. This study can be extended in a few directions as follows:

First, the proposed DMPC-FOA approach is a centralized controller for a CAV platoon. It relies on a single vehicle to compute the optimal control decision. The application of the DMPC-FOA approach for real-time control of the CAV platoon can be constrained by the reserved time τ_2, which is determined by the computational time of the DMPC-FOA approach. To enable controlling a large-size CAV platoon with a large prediction horizon, discretization techniques (e.g., Wei et al., 2017) and a new solution algorithm (e.g, distributed dynamic programming algorithm) will be developed to reduce the computational time for the optimal control problem.

Second, this study does not consider the impacts of uncertainties in system dynamics (e.g., false execution of optimal control, dynamic resistance of the pavement) and initial vehicle conditions (e.g., dynamic communication delays, dynamic sensor measurement errors). However, it is worth noting that the MPC approach has some level of robustness against disturbances in vehicles' states (Zhou et al., 2017). Further, the analytical sensitivity analysis method for the proposed optimal control problem can quantify the impacts of changes in both control decisions and initial vehicle conditions on the CAV

platoon dynamics and the platoon performance. In future work, robust cooperative control strategies will be developed by leveraging the analytical sensitivity analysis method to enable safe and efficient control of the CAV platoon under different levels of uncertainty.

Third, the application of the DMPC-FOA approach depends on two necessary conditions. First, the optimal control decisions are estimated within τ_2 time. Second, the V2V communications are reliable such that the information can be delivered successfully between the leading vehicle and each of the following vehicles. For the cases that one of the two necessary conditions is not satisfied, the ACC or cooperative sensing-based CACC models should be applied immediately to control the car-following behavior of all CAVs. In future, a switching control which leverages the DMPC-FOA approach and the ACC models (or cooperative sensing-based CACC models) will be developed to control the CAV platoon under different traffic flow and communication environments.

Acknowledgements

This study is based on research supported by the Center for Connected and Automated Transportation (CCAT) Region V University Transportation Center funded by the U.S. Department of Transportation (Award #69A3551747105), the Natural Science Foundation of China (71701108), National Science and Technology Major Project (2018YFB1600905), and the K.C. Wong Magna Fund in Ningbo University. Any errors or omissions remain the sole responsibility of the authors.

References

Augustin, D., Maurer, H., 2001. Second order sufficient conditions and sensitivity analysis for the optimal control of a container crane under state constraints. Optimization, 49 (4), 351-368.

Camacho, E. F., Alba, C. B., 2013. Model predictive control. Springer Science & Business Media.

Darbha, S., Rajagopal, K.R., 1999. Intelligent cruise control systems and traffic flow stability. Transportation Research Part C: Emerging Technologies, 7 (6), 329-352.

Desjardins, C., Chaib-draa, B. 2011. Cooperative adaptive cruise control: a reinforcement learning approach. IEEE Transactions on Intelligent Transportation Systems, 12 (4), 1248–1260.

Dorato, P., 1963. On sensitivity in optimal control systems. IEEE Transactions on Automatic Control, 8 (3), 256-257.

Gaimon, C., 2002. Optimal control theory: Applications to management science and economics. JSTOR.

Ge, J. I., Orosz, G.., 2014. Dynamics of connected vehicle systems with delayed acceleration feedback. Transportation Research Part C: Emerging Technologies, 46, 46-64.

Gong, S., Du, L., 2018. Cooperative platoon control for a mixed traffic flow including human drive vehicles and connected and autonomous vehicles. Transportation Research Part B: Methodological, 116, 25-61.

Gong, S., Shen, J., Du, L., 2016. Constrained optimization and distributed computation based car following control of a connected and autonomous vehicle platoon. Transportation Research Part B: Methodological, 94, 314-334.

Hasebe, K., Nakayama, A., Sugiyama, Y., 2003. Dynamical model of a cooperative driving system for freeway traffic. Physical Review E, 68 (2). No.026102.

Jia, D., Lu, K., Wang, J., Zhang, X., Shen, X., 2015. A survey on platoon-based vehicular cyber-physical

systems. IEEE Communications Surveys & Tutorials, 18 (1), 263-284.
Jia, D., Ngoduy, D., 2016. Platoon based cooperative driving model with consideration of realistic inter-vehicle communication. Transportation Research Part C: Emerging Technologies, 68, 245-264.
Keller, H.B., 1976. Numerical solution of two point boundary value problems (Vol. 24). Philadelphia: Society for Industrial and Applied Mathematics.
Kesting, A., Treiber, M., Schonhof, M., Helbing, D., 2008. Adaptive cruise control design for active congestion avoidance. Transportation Research Part C: Emerging Technology, 16 (6), 668–683.
Kirk, D.E., 2012. Optimal control theory: an introduction. Courier Corporation, New York, USA.
Li, Y., Sun, D., Liu, W., Zhang, M., Zhao, M., Liao, X., Tang, L., 2011. Modeling and simulation for microscopic traffic flow based on multiple headway, velocity and acceleration difference. Nonlinear Dynamics, 66 (1-2), 15-28.
Lu, G., Nie, Y.M., Liu, X. and Li, D., 2019. Trajectory-based traffic management inside an autonomous vehicle zone. Transportation Research Part B: Methodological, 120, 76-98.
Malanowski, K., 1984. Differential stability of solutions to convex, control constrained optimal control problems. Applied Mathematics and Optimization, 12 (1), 1-14.
Malanowski, K., 1987. Stability and sensitivity of solutions to optimal control problems for systems with control appearing linearly. Applied Mathematics and Optimization, 16 (1), 73-91.
Malanowski, K., 2011. Sensitivity analysis for state constrained optimal control problems. Control & Cybernetics, 40 (4), 1043-1058.
Malanowski, K., Maurer, H., 1996. Sensitivity analysis for parametric control problems with control-state constraints. Computational Optimization and Applications, 5 (3), 253-283.
Maurer, H., Pesch, H.J., 1994. Solution differentiability for nonlinear parametric control problems. SIAM Journal on Control and Optimization, 32 (6), 1542-1554.
Maurer, H., Pesch, H.J., 1995. Solution differentiability for parametric nonlinear control problems with control-state constraints. Journal of Optimization Theory and Applications, 86 (2), 285-309.
Mayne, D. Q., Rawlings, J. B., Rao, C. V., Scokaert, P. O., 2000. Constrained model predictive control: Stability and optimality. Automatica, 36 (6), 789-814.
Naidu, D.S. 2003. Optimal control systems. CRC Press, Boca Raton, FL, USA.
Nakayama, A., Sugiyama, Y., Hasebe, K. 2001. Effect of looking at the car that follows in an optimal velocity model of traffic flow. Physical Review E, 2001, 65(1).
Ploeg, J., Shukla, D.P., van de Wouw, N., Nijmeijer, H., 2014. Controller synthesis for string stability of vehicle platoons. IEEE Transactions on Intelligent Transportation Systems, 15 (2), 854-865.
Rajamani, R., Shladover, S.E. 2001. An experimental comparative study of autonomous and co-operative vehicle-follower control systems. Transportation Research Part C: Emerging Technologies, 2001, 9(1), 15–31.
VanderWerf, J., Shladover, S. E., Kourjanskaia, N., Miller, M., Krishnan, H., 2001. Modeling effects of driver control assistance systems on traffic. Transportation Research Record, 1748, 167–174.
Wang, M., Daamen, W., Hoogendoorn, S.P., van Arem, B., 2014a. Rolling horizon control framework for driver assistance systems. Part I: Mathematical formulation and non-cooperative systems. Transportation Research Part C: Emerging Technologies, 40, 271-289.
Wang, M., Daamen, W., Hoogendoorn, S.P., van Arem, B., 2014b. Rolling horizon control framework for driver assistance systems. Part II: Cooperative sensing and cooperative control. Transportation

Research Part C: Emerging Technologies, 40, 290-311.
Wang, M., Daamen, W., Hoogendoorn, S.P., van Arem, B., 2016. Cooperative car-following control: Distributed algorithm and impact on moving jam features. IEEE Transactions on Intelligent Transportation Systems, 17 (5), 1459-1471.
Wang, M., Hoogendoorn, S.P., Daamen, W., van Arem, B., Shyrokau, B., Happee, R., 2018. Delay-compensating strategy to enhance string stability of adaptive cruise controlled vehicles. Transportmetrica B: Transport Dynamics, 6 (3), 211-229.
Wang, Y., Li, X., Yao, H. 2019. Review of trajectory optimisation for connected automated vehicles. IET Intelligent Transport Systems, 13 (4), 580-586.
Wei, Y., Avcı, C., Liu, J., Belezamo, B., Aydın, N., Li, P.T. and Zhou, X., 2017. Dynamic programming-based multi-vehicle longitudinal trajectory optimization with simplified car following models. Transportation Research Part B: Methodological, 106, 102-129.
Zheng, Y., Eben Li, S., Wang, J., Cao, D., Li, K. 2016. Stability and scalability of homogeneous vehicular platoon: study on the influence of information flow topologies. IEEE Transactions on Intelligent Transportation Systems, 17(1), 14–26.
Zhou, Y., Ahn, S., Chitturi, M., Noyce, D.A., 2017. Rolling horizon stochastic optimal control strategy for ACC and CACC under uncertainty. Transportation Research Part C: Emerging Technologies, 83, 61-76.